

Experimental modal analysis of the H-drive

Citation for published version (APA):

Merry, R. J. E. (2003). *Experimental modal analysis of the H-drive*. (DCT rapporten; Vol. 2003.078). Technische Universiteit Eindhoven.

Document status and date:

Published: 01/01/2003

Document Version:

Publisher's PDF, also known as Version of Record (includes final page, issue and volume numbers)

Please check the document version of this publication:

- A submitted manuscript is the version of the article upon submission and before peer-review. There can be important differences between the submitted version and the official published version of record. People interested in the research are advised to contact the author for the final version of the publication, or visit the DOI to the publisher's website.
- The final author version and the galley proof are versions of the publication after peer review.
- The final published version features the final layout of the paper including the volume, issue and page numbers.

[Link to publication](#)

General rights

Copyright and moral rights for the publications made accessible in the public portal are retained by the authors and/or other copyright owners and it is a condition of accessing publications that users recognise and abide by the legal requirements associated with these rights.

- Users may download and print one copy of any publication from the public portal for the purpose of private study or research.
- You may not further distribute the material or use it for any profit-making activity or commercial gain
- You may freely distribute the URL identifying the publication in the public portal.

If the publication is distributed under the terms of Article 25fa of the Dutch Copyright Act, indicated by the "Taverne" license above, please follow below link for the End User Agreement:

www.tue.nl/taverne

Take down policy

If you believe that this document breaches copyright please contact us at:

openaccess@tue.nl

providing details and we will investigate your claim.

Experimental modal analysis of the H-drive

R.J.E. Merry

Report No. DCT 2003.78

Report of internal traineeship

Coach: ir. M.G.E. Schneiders

Advisor: ir. P.W.J.M. Nuij

Supervisor: prof.dr.ir. M. Steinbuch

Eindhoven University of Technology (TU/e)
Department of Mechanical Engineering
Control Systems Technology Group

Eindhoven, September 10, 2003

Abstract

Controller design is often based on a measured Frequency Response Function (FRF) of a system. The eigenmodes present in the servo FRF can limit the bandwidth or the performance of the controlled system. By performing a modal analysis of the system the eigenmodes can be given a physical interpretation and a model of the dynamic behaviour of the system is derived. The problem definition of this traineeship is defined as:

Perform an experimental modal analysis of the H-drive in order to obtain the modal parameters of the modes of the system that limit its performance.

To get familiar with the measurement method a modal analysis of a simple beam structure is performed before the modal analysis of the H-drive is carried out. The position dependency of the eigenmodes of the H-drive is investigated by performing a modal analysis with the H-drive in an other configuration.

For the modal analysis the H-drive is excited with an impulse hammer on a grid of points and the resulting acceleration is measured at a fixed point. On the resulting calculated FRFs a fit is performed to obtain the modal parameters. The modal parameters are the modal frequency, the modal damping and mode shape. A driving point measurement can be done by exciting the system at the same point where the acceleration is measured. This driving point measurement can be used to check the quality of the measurement loop and to scale the mode shapes to Unit Modal Mass.

For the modal analysis of the beam structure, measurement points are chosen both in and outside the line of the heart of the beam. This enables measurement of torsional modes. Since resonance frequencies are global parameters of a system, the various resonances of the measured FRFs have matching frequencies. By fitting the resonances with the global polynomial method, the modal parameters are derived. The resulting mode shapes are both bending and torsional modes.

The H-drive consists of two parallel moving y motors which drive a x motor on a beam in between. The servo FRF of the x motor contains several eigenmodes. For each part a set of modal FRFs is measured. The eigenmodes present in the servo FRF can be ascribed to resonances of the different parts by matching resonance frequencies. The resonances of interest can be fitted to obtain the modal parameters. The outcome of the fit is that the eigenmodes of the servo FRF are caused by resonances of the beams in y direction, the beam in x direction and the head on the beam in x direction.

The resonance frequencies vary for servo measurements in other configurations. The modal parameters can be position dependent. Most modes are present in the beam in x direction and its head. Therefore only the x position of the head is changed for the second modal analysis. The resonances of the servo FRF of the second configuration are caused by the same modes of the same parts. However some resonances shift in frequency when the configuration is changed. One resonance of the second modal analysis is not visible in the first configuration. This is because the head on the x beam is placed at a position where the mode has no component in the direction of the servo measurement.

With the knowledge obtained by the mode shapes the system can be optimized in order to improve the performance of the controlled system.

Contents

Abstract	i
1 Introduction	1
1.1 Overview	1
1.2 Goal	1
1.3 Outline	2
2 Theory	3
2.1 Fourier transform	3
2.1.1 Signal leakage	4
2.1.2 Aliasing	5
2.2 Frequency response functions	6
2.2.1 Power spectra	6
2.2.2 Identification	7
2.3 Fit procedure	7
2.3.1 Frequency and damping	8
2.3.2 Residues	8
2.3.3 Effective mass, stiffness and damping	9
3 Experimental aspects	11
3.1 Measurement method	11
3.2 Sensors	11
3.2.1 Impact hammer	11
3.2.2 Accelerometer	12
3.2.3 Calibration	12
3.3 Measuring	13
3.3.1 Measurement points	13
3.3.2 Triggering	14
3.3.3 Windows	14
3.3.4 Averaging	14
3.3.5 Frequency range	15
3.3.6 Voltage range	15
3.3.7 Reproducibility	15
3.3.8 Driving point measurements	15
4 Modal analysis beam	17
4.1 The beam structure	17
4.2 Experiments	17
4.2.1 Measurement points	18
4.2.2 Hammer tip	18
4.2.3 Settings FRF analyzer	18
4.2.4 Driving point measurements	19

4.2.5	Reproducibility	20
4.2.6	Modal measurements	20
4.3	Results	21
4.3.1	Modal parameters	21
4.3.2	Mode shapes	22
4.3.3	MAC values	23
5	Modal analysis H-drive	25
5.1	The H-drive	25
5.2	Servo measurements	26
5.3	Experiments	26
5.3.1	Measurement points	27
5.3.2	Hammer tip	28
5.3.3	Settings FRF analyzer	28
5.3.4	Driving point measurements	28
5.3.5	Reproducibility	28
5.3.6	Modal measurements	29
5.4	Comparing FRFs	30
5.5	Results	33
5.5.1	Mode shapes	33
5.5.2	MAC values	35
6	Position dependency	37
6.1	Servo measurements	37
6.2	Modal experiments	38
6.2.1	Modal measurements	39
6.2.2	Comparing FRFs	40
6.3	Results	43
6.3.1	Mode shapes	43
6.3.2	MAC values	45
6.4	Comparing configurations	45
7	Conclusion	49
7.1	Recommendations	50
	Bibliography	51
A	Coordinates beam structure	53
B	Modal parameters beam structure	55
B.1	Z direction	55
B.2	Y direction	58
C	Mode shapes beam structure	59
C.1	Shapes z direction	59
C.2	Shapes y direction	60
D	Coordinates configuration 1	61
D.1	Coordinates Xbeam	61
D.2	Coordinates Xhead	62
D.3	Coordinates Ybeam	62
D.4	Coordinates Yhead	63
E	Coordinates configuration 2	65
E.1	Coordinates Xhead	65

F	Modal parameters H-drive conf 1	67
F.1	X direction Xbeam	67
F.2	Y and z direction Xbeam	68
F.3	Xhead	69
F.4	Y1beam	70
F.5	Y2beam	70
G	Mode shapes H-drive conf 1	71
H	Modal parameters H-drive conf 2	73
H.1	X direction Xbeam	73
H.2	Y and z direction Xbeam	74
H.3	Xhead	75
H.4	Y1beam	76
H.5	Y2beam	76
I	Mode shapes H-drive conf 2	77

Chapter 1

Introduction

For control purposes the design of a controller is often based on a measured Frequency Response Function (FRF) of a system. This FRF can contain a number of resonances which can limit the achievable bandwidth or the performance of the controlled system. The resonances in the FRF are caused by modes of the system and are therefore called the eigenmodes of the system. Modes let structures act as mechanical amplifiers. At certain natural frequencies of the structure, the modal frequencies, a small amount of input force can cause a very large response. The question arises what causes these eigenmodes. In other words, what mode shapes, in which part of the structure, cause the resonances to appear in the FRF. These mode shapes, together with the modal frequency and modal damping, can be obtained by a modal analysis. This report deals with the modal analysis of an H-drive. A general outline of modal analysis is presented in Section 1.1. The goal of the project is described in Section 1.2 and the overview of the report is given in Section 1.3.

1.1 Overview

Modal analysis is an experimental procedure to investigate the dynamical behaviour of a mechanical system. In recent years there has been a considerable interest in the dynamic behaviour of mechanical systems. The identification of the kinematic and dynamic parameters of systems are essential for an accurate description of the systems dynamic characteristics. When the dynamic behaviour of a system is known, the design of a controller of the system for various purposes can be based on this knowledge. Many parameter estimation procedures, both analytical and experimental, are established. These include e.g., estimation using rigid body models, dynamic modelling techniques, adaptive control, modal analysis, etc.

For weakly damped systems, each mode of a mechanical system can be considered as an independent single-degree-of-freedom system. The dynamic response of a system can be written as a linear superposition of the independent single-degree-of-freedom modal responses. The derivation and use of the system model based on resonance frequencies, damping ratios and mode shapes is the essence of modal analysis. With a modal analysis the modal parameters, modal frequency, modal damping and the mode shape of a system are obtained experimentally. They can be given a direct physical interpretation. With the results of the modal analysis, design improvements can be predicted and the structure can be optimized. The design improvements incorporate the change of the mass or the stiffness of the system, or the addition of an extra actuator in order to improve the controlled behaviour of the system.

1.2 Goal

The system under consideration for this project is a so called H-drive. The eigenmodes of the system limit the performance of the controlled system. With experimental modal analysis, the

modal frequencies, modal damping and the mode shapes of the eigenmodes of the H-drive can be obtained. If the modal parameters of the eigenmodes that limit the performance of the system are known, changes to the controlled system can be made to improve the performance. The problem definition of this report is defined as:

Perform an experimental modal analysis of the H-drive in order to obtain the modal parameters of the modes of the system that limit its performance.

In order to perform the experimental modal analysis, first the necessary theory must be studied. Furthermore the different experimental aspects that are important to perform good measurements must be considered. To get familiar with the method of testing and the interpretation of the obtained results, the procedure of modal analysis is first tested on a relatively simple beam structure. With the acquired experience, a modal analysis of the H-drive is performed. Furthermore the position dependency of the modal parameters is tested. The testing is done by performing servo measurements and two separate modal analyses with the parts of the H-drive at a different position. By comparing the results of the two modal analyses, the position dependencies of the results become clear.

1.3 Outline

The concept of modal analysis is described in more detail in Chapter 2, together with the theory needed to perform modal analysis. The experimental aspects of the modal analysis, such as the measurement method, the used sensors and other measurement aspects are dealt with in Chapter 3. The modal analysis of the beam structure is the subject of Chapter 4. The modal analysis of the H-drive will be discussed in Chapter 5. The eigenmodes are ascribed to mode shapes of the various parts of the H-drive by comparing the modal measurements to servo measurements. The servo measurements and the comparison are also treated in Chapter 5. Chapter 6 describes the testing of the global usefulness of the results obtained by the modal analysis. Finally conclusions will be drawn and recommendations for further research are given in Chapter 7.

Chapter 2

Theory

The dynamic behaviour of structures or robots can be obtained through experimental modal analysis. This technique consists of applying a known excitation to a structure and measuring its response, in this case an impact excitation by a hammer. The excitation can also be done by for instance a shaker. The impact excitation by the hammer is like a delta-function, which contains all frequencies with uniform amplitude. The hammer impact tends to accentuate the non-linearities of the structure [5]. The bandwidth of the excitation spectrum is limited by the material of the tip of the hammer and by the mass of the hammer. The response of the structure is measured with an accelerometer. The structure is discretized by means of a grid of measurement locations. The locations of these measurement points must be chosen in such a way that the representation is accurate enough. Too many points make the testing and analysis process time consuming. Too few points will not provide a suitable representation. The accelerometer is mounted at a fixed point, while the excitation of the system is exerted at different measurement points. The experimental considerations will be discussed in more detail in Chapter 3.

The time signals of the excitation in each point and its response are converted to the frequency domain using the Fourier transform. Errors in the conversion are introduced by signal-leakage and aliasing. The effect of both error sources is reduced as much as possible. Using the auto power spectrum and the cross power spectrum, the frequency response function (FRF) can be calculated between the measurement point and the excitation point. The coherence function is calculated to check the quality of the measurements. Through a fitting procedure a model is calculated that describes the response of the system. This model is expressed with modal frequencies, modal damping coefficients and complex residues. The residues are also called mode shapes.

The Fourier transform, signal leakage, aliasing, the calculation of the spectra and the fit procedure will be further explained in this chapter. The measurement of the time signals and the Fourier transform are performed by a Siglab analyzer. For the postprocessing of the data and the fit procedure ME'scope is used [13].

2.1 Fourier transform

The excitation and response are measured as a function of time. These time-signals are obtained using a discrete sampling time. Therefore the discrete Fourier transform (DFT) must be used. The signals are recorded over a time interval $0 \leq t \leq T$ and digitized using fixed time-steps T_s . With the fixed time-steps the total measurement time T is divided into N equal intervals. The sample frequency is defined as $f_s = 1/T_s$. The discrete Fourier transformation $X[n]$ of a discrete signal $x[k]$, where $k = 0, 1, \dots, N$, is defined by Eq. 2.1. The inverse discrete Fourier transform is

shown in Eq. 2.2.

$$X[n] = \frac{1}{N} \sum_{k=0}^{N-1} x[k] e^{-2\pi jkn/N}, \quad n = 0, 1, \dots, N-1 \quad (2.1)$$

$$x[k] = \sum_{n=0}^{N-1} X[n] e^{2\pi jkn/N}, \quad k = 0, 1, \dots, N-1 \quad (2.2)$$

As an example, the discrete Fourier transform of a window function (see Fig. 2.1) is calculated. The measuring time T is 100 s, the fixed time-step $T_s = 0.5$ s. So the total measurement time T is divided into $N = 200$ intervals. The sample frequency is $f_s = 2$ Hz, the spectral distance $\Delta f = f_s/N = 0.01$. The resulting DFT is shown in Fig. 2.2, in this figure can be seen that the DFT folds around $\frac{1}{2}f_s$.

The calculation of the Fourier transform is done by Siglab. The implemented algorithm in the Siglab analyzer is the Fast Fourier Transform (FFT) [7]. The FFT algorithm is more effective with respect to the calculational costs.

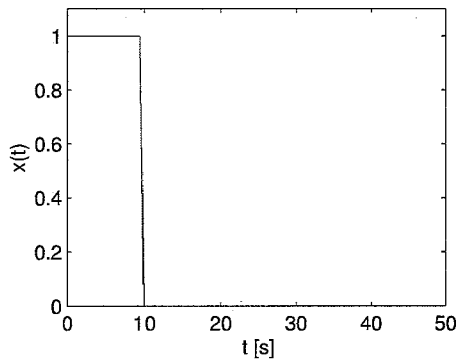


Figure 2.1: rectangular window

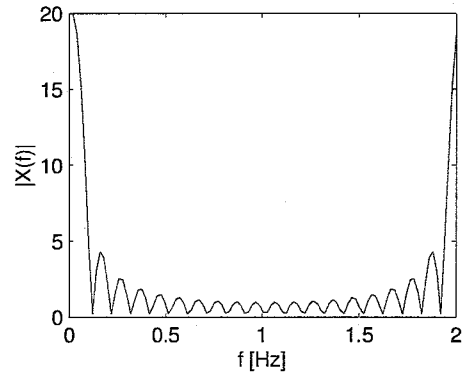


Figure 2.2: DFT rectangular window

2.1.1 Signal leakage

When a signal is recorded using discrete sampling, there are two parameters which control the accuracy of the calculated spectrum through FFT or DFT. The first is the sample frequency f_s , or the sample rate $T_s = 1/f_s$. The second is the number of samples N , or the length of the time interval T .

The finite time interval introduces signal leakage. To evaluate this, it is assumed that the signal $x_W(t)$ over a time interval $0 \leq t \leq T$ is calculated by multiplying the original signal $x(t)$ with a rectangular window $w(t)$. The window $w(t)$ has the value 1 in the interval $0 \leq t \leq T$ and has the value 0 outside this interval. So the windowed signal $x_W(t)$ can be written as $x_W(t) = x(t)w(t)$. The multiplication of two signals in the time domain leads to a convolution product in the frequency domain [7], [6], [4]. The transformation of $x_W(t)$ to the frequency domain leads to:

$$X_W(f) = W(f) \otimes X(f) = \int_{-\infty}^{\infty} W(\varphi) X(f - \varphi) d\varphi \quad (2.3)$$

The wanted Fourier transform is $X(f)$, but because of the finite time interval the approximation $X_W(f)$ is calculated. The Fourier transform of the rectangular window described before is:

$$W(f) = T \frac{\sin(\pi f T)}{\pi f T} e^{-\pi j f T} \quad (2.4)$$

The Fourier transform of the rectangular window is shown in Fig. 2.2. The convolution of $X(f)$ with $W(f)$ leads to a kind of spreading of the frequency content of $X(f)$. Therefore dummy frequencies appear because of the window. This spreading is called signal leakage.

For the calculation of the DFT, the windowed part of the signal $x(t)$ is copied and shifted an infinite number of times. Discontinuities can arise at the edges of the windowed parts when the shifting does not produce a smooth function.

So the two main causes for signal leakage are the choice of the window function and the edge discontinuities. Some examples of window functions that reduce the edge discontinuities and causes less spreading are the Hanning-, the Blackman-, Hamming- and the Kaiser-window. These windows are displayed in the time domain in Fig. 2.3 over a time interval of $0 \leq t \leq 50$ seconds. Except for the rectangular-window, these window-functions are small or zero at the edges to reduce the edge discontinuities.

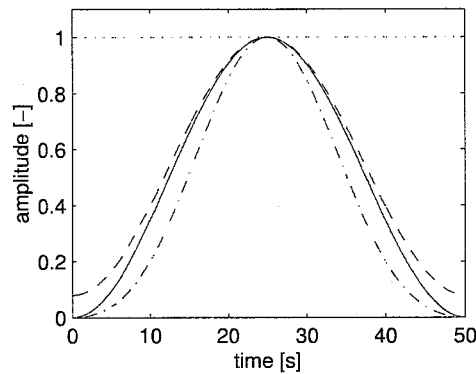


Figure 2.3: windows: rectangular (dotted), Hanning (solid), Hamming (dashed) and Blackman (dash-dotted)

2.1.2 Aliasing

The sampling frequency f_s is defined as $f_s = 1/T_s$, with T_s the time between two samples. The highest frequency which appears in a signal is defined as f_{max} .

If f_{max} is greater than $f_s/2$, frequencies between $f_s/2$ and f_{max} are folded back in the spectrum around $f_s/2$. These frequencies appear as a lower frequencies in the spectrum. This phenomenon is called aliasing. See also [7], [6], [4], [2].

To prevent the loss of information of $X(f)$, thus to prevent aliasing, the folding frequency should be greater than the maximum frequency which appears in the original signal. This folding frequency is also called the Nyquist frequency f_{Nyq} and is defined as:

$$f_{Nyq} = \frac{f_s}{2} > f_{max} \quad (2.5)$$

Signals with frequencies lower than the Nyquist frequency are accurately sampled. Signals with frequencies greater than f_{Nyq} are not accurately sampled, the frequencies above the Nyquist frequency incorrectly appear as lower frequencies in the spectrum.

From the theorem of Shannon it can be concluded that there is no loss of information when the sample frequency is at least two times higher than the highest frequency which appears in a signal [7].

An example of aliasing is shown in Fig. 2.4. This figure shows a harmonic signal $x(t) = \sin(2\pi 5t)$ in the upper graph. The highest frequency in this signal is 5 Hz. This signal is sampled with a sample frequency of $f_s = 8$ Hz, the sample points are shown in the middle graph. When a sine-function is fitted through the measured data, a sine-function of 3 Hz appears, this signal is shown in the lowest graph. The Nyquist frequency is $f_{Nyq} = 4$ Hz. The frequency of 5 Hz folds around the Nyquist frequency and appears as a frequency of $4 - (5 - 4) = 3$ Hz.

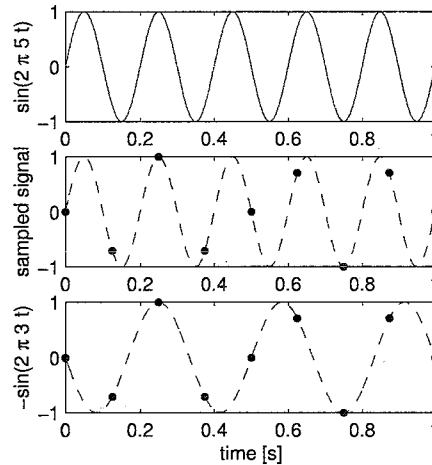


Figure 2.4: aliasing of $x(t) = \sin(2\pi 5t)$ with $f_s = 8$ Hz

2.2 Frequency response functions

The recorded time signals have been transformed to the frequency domain using Fourier transformation. The frequency response functions can be calculated using the auto power spectrum $S_{xx}(f)$ and the cross zonnenspectrum $S_{xy}(f)$. The calculation of both spectra and the calculation of the FRF are the subject of this section.

2.2.1 Power spectra

When a signal $x(t)$ is windowed over a time interval $0 \leq t \leq T$ the Fourier transform of the windowed signal $x_W(t)$ can be calculated, as explained in the previous section. With the Fourier transform $X_W(f)$ the auto power spectrum can be calculated using Eq. 2.6. The auto power spectrum and the auto correlation function together form a Fourier transformation. More information about the correlation function and its relation to the spectra can be found in [7] and [8].

$$S_{xx}(f) = \frac{1}{T} X_W^*(f) X_W(f) \quad (2.6)$$

In Eq. 2.6 * denotes the complex conjugate. The auto power spectrum is a real, symmetric function and has a non-zero average. The auto power spectrum provides information about the frequencies present in a signal and the contribution of each component to the total power in the signal. When the signal $x(t)$ is a random signal, for instance due to the presence of noise, an averaging procedure can be used to get an accurate estimation of $S_{xx}(f)$. For this purpose the Fourier transform is calculated a number of times. The mean of the auto power spectrum of each of the Fourier transforms is calculated.

When a second signal $y(t)$ is introduced the cross power spectrum $S_{xy}(f)$ can be calculated between the signals $x(t)$ and $y(t)$. The signal $x(t)$ is the excitation signal and $y(t)$ is the measured response of a system. The cross power spectrum is defined in Eq. 2.7.

$$S_{xy}(f) = \frac{1}{T} X_W^*(f) Y_W(f) \quad (2.7)$$

In contrast to the auto power spectrum, the cross power spectrum is a complex function. Furthermore the cross power spectrum has a kind of symmetry by $S_{xy}(f) = S_{yx}^*(f)$. Again for random signals an estimation can be found by averaging a number of cross power spectra of the signals.

2.2.2 Identification

Using the auto power spectrum and the cross power spectrum, the frequency response function can be calculated using Eq. 2.8.

When the cross power spectrum is normalized using the corresponding auto power spectra, this leads to the coherence function $\gamma_{xy}^2(f)$. The coherence function is defined in Eq. 2.9. The coherence function is a normalized coefficient of correlation between the excitation signal $x(t)$ and the response signal $y(t)$ evaluated at each frequency.

$$H_{xy}(f) = \frac{S_{xy}(f)}{S_{xx}(f)} \quad (2.8)$$

$$\gamma_{xy}^2(f) = \frac{|S_{xy}(f)|^2}{S_{xx}(f) S_{yy}(f)} \quad (2.9)$$

The coherence function $\gamma_{xy}^2(f)$ provides information for each frequency which part of the output $y(t)$ is caused by the input $x(t)$ and which part is due to noise $n(t)$. Since $S_{nn}(f) < S_{yy}(f)$, the range of the coherence function is $0 \leq \gamma_{xy}^2(f) \leq 1$. If $\gamma_{xy}^2(f)$ is close to 1 a big relation exists between the input and output. If $\gamma_{xy}^2(f)$ is near 0 the output is dominated by the noise. The coherence function can have a lower value near an anti-resonance. Near an anti-resonance the system has less energy in the auto power spectrum, therefore the input-output relation is smaller. This results in a lower coherence value.

If the signals are random, estimations for the frequency response function and the coherence can be made by averaging, as was the case for the spectra.

2.3 Fit procedure

When the frequency response functions (FRFs) have been calculated using the methods explained in Sections 2.1 and 2.2, the modal parameters can be estimated using a curve fitting procedure. With this procedure the modal parameters are extracted from the measured data. The modal parameters are the modal frequency, modal damping and complex residue (also called mode shape).

The curve fitting method used in this project is the Global Polynomial method. This method is a frequency domain curve fitting method for a specified frequency cursor band. It is able to find closely coupled modes. The global polynomial method is a Multi-Degree-Of-Freedom (MDOF) method that can simultaneously estimate the modal parameters of two or more modes. It uses the Rational Fraction Polynomial (RFP) curve fitting algorithm. [9] The RFP algorithm is a MDOF method that fits an analytical expression to a FRF measurement. It fits the FRFs in a least-squared error sense. During the fit the coefficients of the numerator and denominator polynomials are identified. The analytical form used for the fit is the Rational Fraction Form, it is shown in Eq. 2.10. The RFP algorithm can handle noisy measurements because of the least-squared error formulation. More important, it offers a way of handling the residual effects of out-of-band modes by allowing additional numerator polynomial terms. [13]

$$H(\omega) = \frac{\sum_{k=0}^m a_k s^k}{\sum_{k=0}^n b_k s^k} \Bigg|_{s=j\omega} \quad (2.10)$$

Errors during the fitting proces are reduced by dividing it up into two steps:

1. the estimation of the frequency and damping parameters
2. the estimation of the residues

The Global Polynomial method has several advantages. First more accurate frequency and damping estimates can be obtained by processing all of the measurements than can be obtained

from curve fitting a single measurement. A second advantage is that the residues are estimated more accurately during the second step, because the damping is already known and fixed in the first step.

There are also some disadvantages. If the modal frequency or damping vary substantial from one measurement to another, the global method will be in error. The global method assumes that these parameters are unchanging. An other disadvantage is that the accuracy of the residue estimates depends on the accuracy of both the global frequency and damping estimates.

The Global Polynomial method is chosen over the CoQuad and Peak method [13] because the last two methods do not estimate the modal damping. The Complex Exponential method [13] is also a MDOF method that can simultaneously estimate the modal parameters of two or more modes. It uses the Least Squares Complex Exponential (LSCE) algorithm. The Complex Exponential method works best on wider frequency bands, using one or more extra computational modes than the number of modal peaks present in the cursor band. The Polynomial method works better in small frequency bands in the vicinity of resonance peaks, using a small number of modes. Because the modal peaks are selected visually one at a time, the Polynomial method is used.

The FRF matrix can be written in partial fraction form, which is shown in Eq. 2.11.

$$[H(\omega)] = \sum_{k=1}^{\text{modes}} \left[\frac{[R(k)]}{j\omega - p(k)} + \frac{[R^*(k)]}{j\omega - p^*(k)} \right] \quad (2.11)$$

where

- $[H(\omega)] = \text{FRF matrix}$
- $\omega = \text{frequency variable (radians/second)}$
- $p(k) = \text{pole location for the } k^{\text{th}} \text{ mode} = -\sigma(k) + j\omega(k)$
- $\sigma(k) = \text{modal damping for the } k^{\text{th}} \text{ mode (radians/second)}$
- $\omega(k) = \text{modal frequency for the } k^{\text{th}} \text{ mode (radians/second)}$
- $[R(k)] = \text{residue matrix for the } k^{\text{th}} \text{ mode (n by n)}$
- $n = \text{number of DOFs of the FRF model}$
- $\text{modes} = \text{number of modes of interest on the structure}$
- * – denotes the complex conjugate

2.3.1 Frequency and damping

In the first step of the curve fitting process, the modal frequency and damping are estimated. The frequency of a resonance peak in the FRF is used as the modal frequency. This peak frequency, which is also dependent on the frequency resolution of the measurements, is not exactly equal to the modal frequency, but is a close approximation. The resonance peak should appear at the same frequency in almost every FRF measurement. The resonance peak will not appear in FRFs of points on nodal lines of the mode shape.

Note that the denominators of each term of the FRF matrix of Eq. 2.11 are the same. The denominators only depend on the pole location of each mode. The Global Polynomial method performs a least squared error curve fit of multiple FRFs and estimates the coefficients of the FRF denominator polynomial. The FRF denominator polynomial is called the characteristic polynomial. The modal frequency and damping estimates are extracted as roots of the characteristic polynomial.

2.3.2 Residues

Once the modal frequency and damping are estimated in the first step, the modal residues are estimated in the second step. The numerator terms in the FRF model consist of a pair of (n

by n) matrices, the residue matrix and its conjugate. Each mode k has a residue matrix $[R(k)]$ associated with it. Each residue matrix has the same dimensions as the FRF matrix.

During the residue curve fitting step, the numerator polynomial of each FRF is estimated by a least squared error curve fitting process. The residual effects of out-of-band modes are compensated for by the use of additional numerator polynomial terms. Each modal residue estimate is determined by a partial fraction expansion of the polynomial form of the FRF. Because the out-of-band modes are compensated for, the cursor bands do not need to overlap or cover the whole frequency band.

If a driving point measurement is present, the mode shapes can be scaled to Unit Modal Mass (UMM). The driving point measurements will be discussed further in Section 3.3.8.

To quantitatively compare the fitted mode shapes, the Modal Assurance Criterion (MAC) can be used. MAC values vary between 0 and 1, they indicate whether or not two shapes are the same. The MAC is computed between two complex shape vectors ($\{X\}, \{Y\}$) using the following formula, where $*$ denotes the transposed complex conjugate vector. [13]

$$MAC(\{X\}, \{Y\}) = \frac{\|\{X\}^* \{Y\}\|^2}{\|\{X\}\| \|\{Y\}\|} \quad (2.12)$$

MAC values can be interpreted as follows:

- MAC = 0 to 0.9 - the two mode shapes are different
- MAC > 0.9 - the two mode shapes are similar
- MAC = 1.0 - the two mode shapes are identical

2.3.3 Effective mass, stiffness and damping

With the modal parameters, the effective mass, damping and stiffness can be calculated. The effective mass, damping and stiffness of each mode are the values each mode would have if it were a single Mass-Spring-Damper system. The effective mass m_{eff} can be calculated using Eq. 2.13, the effective damping d_{eff} using Eq. 2.14 and the effective stiffness k_{eff} can be calculated using Eq. 2.15. These formulas use the frequency $f = \frac{\omega_r}{2\pi}$, with ω_r the resonance frequency in rad/s, the damping d and the residue r . The residue r is a component of the residue matrix R by $r = R_{ij}(k)$ for each mode k . $Re(r)$ is the Real part of the residue and $Im(r)$ is the Imaginary part of the residue. [13]

$$m_{eff} = \frac{1}{(f \cdot Re(r) + d \cdot Im(r))} \quad (2.13)$$

$$d_{eff} = 2 \cdot d \cdot m_{eff} \quad (2.14)$$

$$k_{eff} = (f^2 + d^2) \cdot m_{eff} \quad (2.15)$$

Chapter 3

Experimental aspects

The theoretical background needed for modal analysis is explained in Chapter 2. This chapter deals with the considerations and issues needed for the experimental part of the modal analysis. First a global explanation of the experimental tools will be discussed. The specifications of the sensors, needed for the measuring of the signals, are described next. When the tools needed for the experimental modal analysis are discussed, the choice of the measurement points is treated, together with the most important settings for the FRF analyzer Siglab. Finally some specific measurements for quality control are discussed.

3.1 Measurement method

For modal testing the FRFs of at least one row or column of the total FRF matrix are required. The FRF matrix consists of the FRFs between all the measurement points of the structure. The rows of the FRF matrix contain the FRFs for a fixed output and multiple inputs. The columns of the FRF matrix contain the FRFs for multiple outputs and a fixed input. [10] The first corresponds to a roving hammer impact test, the second is typical a shaker test. Because the H-drive is difficult to excite with a shaker, the experimental modal analysis of this report is done with a impact hammer. So the rows of the FRF matrix are measured. During the experiments the impact exerted on and the acceleration of the structure are measured. The impact is measured directly by the roving hammer and the acceleration by an accelerometer.

The accelerometer is the fixed output and the input of the roving hammer moves from point to point. The fixed output is called the reference. This type of testing is called single reference testing.

3.2 Sensors

The FRFs are computed by a Siglab analyzer using the measured impact of the hammer and the measured resulting acceleration of the structure. The specifications of the sensors are described in this section. The calibration of the accelerometer and the testing of the sensors with a known mass are also treated in this section.

3.2.1 Impact hammer

The used impact hammer from 'PCB piezotronics' had a build in quartz force sensor in order to measure the impact. Table 3.1 gives the specifications of the used hammer.

In Siglab the sensitivity of the impact signal is specified in N/V, so the hammer sensitivity is approximately 435 N/V. The quartz force sensor needs power supply to work. This power is applied through the same cable as where the force is measured. This is done in Siglab by giving the hammer a bias. Because of the bias it is only possible to measure the force by AC, the DC

Max frequency range	8 kHz
Hammer range (for 5 V output)	440 N
Hammer sensitivity	2.3 mV/N
Resonant frequency	31 kHz
Hammer mass (without extender)	0.14 kg

Table 3.1: specifications impact hammer

part is used for the power supply. With the AC part, it is not possible to measure signals at low frequencies, up to approximately 0.1 Hz.

3.2.2 Accelerometer

For the measurement of the acceleration, an ‘Kistler’ accelerometer, type 8628 B50, is used. The accelerometer as a built-in charge amplifier and low-impedance voltage output. The accelerometer also needs a bias in Siglab. The specifications of the accelerometer are given in Table 3.2.

Range	± 50 g
Sensitivity ($\pm 5\%$)	100 mV/g
Mass	6.7 g
Resonant frequency	22 kHz

Table 3.2: specifications accelerometer

In Siglab the sensitivity of the accelerometer is defined in $\text{m/s}^2/\text{V}$. So the sensitivity of the used accelerometer is approximately $98.12 \text{ m/s}^2/\text{V}$, with the gravitational constant $g = 9.812 \text{ m/s}^2$. In the measurement setup menu from Siglab the sensitivity of the accelerometer can be changed to V/units in stead of units/V .

3.2.3 Calibration

The accelerometer is calibrated using a shaker and a calibrated accelerometer. The calibration is done by determining the FRF between the two measured accelerations of both accelerometers. The input for the experiment is a chirp¹ signal. The two accelerometers should respond the same to the input signal, so the FRF between the two signals should have an amplitude of 1 (0 dB) for all frequencies. During the first experiment, the amplitude of the FRF for the not calibrated accelerometer had a value of 0.95, so the sensitivity of the accelerometer is changed by 5%, to $103 \text{ m/s}^2/\text{V}$, in order to get the amplitude of the FRF 1 for all frequencies.

The sensitivities of both the hammer and accelerometer can be used in Siglab to display the responses in engineering units.

The combination of accelerometer and impact hammer is tested using a block with known mass. The accelerometer is placed at one end of the block and the total of block and accelerometer is hung in a tripod using two ropes. With the hammer a force is applied to the end of the block where no accelerometer is placed. The force and acceleration are measured by Siglab. The FRF between these two signals can be calculated and is shown in Fig. 3.1.

Because the system consists of a single mass, the formula $F = ma$ is valid. The amplitude of the bodeplot of a single mass should be a straight line for all frequencies at an amplitude of $1/m$. The phase should be 0° or -180° , depending on the orientation of the accelerometer. If the amplitude of the FRF is not equal to $1/m$, the sensitivity of the accelerometer or the hammer can be adjusted until the right mass is measured. The measured mass can vary within the range of accuracy of the sensors.

¹A chirp signal is a sinusoidal signal with increasing frequency.

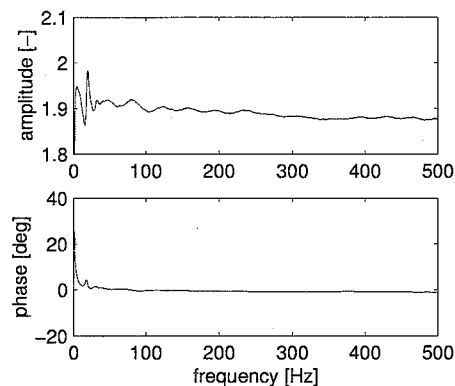


Figure 3.1: bodeplot of measured block

The block used for the experiment has a mass of 532 g, the accelerometer has a mass of 6.7 g, so the total mass of the system is 538.7 g. The parameters of the modal windows used for the experiment are given in Table 3.3. More information about the use of these windows can be found in Section 3.3.3.

Double hit amplitude	50 %
Double hit delay	20 %
Force window size	7 %
Exponential window decay	10 %

Table 3.3: parameters modal windows

The amplitude of the measured FRF shown in Fig. 3.1 is around 1.9, the measured mass $m = 1/1.9 \text{ kg} = 0.5263 \text{ kg} = 526.3 \text{ g}$. The real mass is 538.7 g. The measured mass has an error of 2.3%. This error lies within the deviation of the accelerometer of $\pm 5 \%$. The amplitude of Fig. 3.1 shows a slope different from 0 and a phase different from 0 for low frequencies. The oscillations in the FRF are likely to be caused by the rectangular window used for the force signal (see research done by Mathijs Cuijpers). Furthermore, because of the bias, needed to power the sensors, the measurements for low frequencies, up to 0.1 Hz, are unreliable.

3.3 Measuring

The quality of the measurements depends on the skills of the person performing the experiments, the used sensors, data-acquisition devices, etc. The settings of the data-acquisition device, Siglab, also influence the accuracy of the measurements. This section deals with considerations and settings that can improve the accuracy.

3.3.1 Measurement points

During a roving impact hammer test the accelerometer is the reference signal and remains on a fixed location, as stated in Section 3.1. With the hammer a force is applied on the structure at several locations. The choice of the locations for the measurement points depends on the kind of modes that want to be visualized. The number of measurement points should be the lowest one which best represents the modes under study. Too many points make the testing and analysis process time consuming. Too few locations will not provide a suitable representation of the modes, this phenomenon is called spatial aliasing.

The points of excitation and the location of the accelerometer can be numbered. These numbers can be used as the channel labels of Siglab, along with the direction of the sensors. The coordinates of the measurement points can be used to implement the points in a structure file in ME'scope [13], the same numbers can be attributed to the corresponding points in ME'scope. By number matching the measurement data can easily be attributed to the various points.

The resonance frequencies in the calculated FRFs are the same for each location and are global parameters of a structure. The amplitude and phase however can change from location to location and are local parameters that depend on the location of the points. When a resonance is not visible in a point, the location of the accelerometer and hammer can lie in a node of the mode shape.

3.3.2 Triggering

In the sampling window of Siglab, the exerted force and the resulting accelerations of the structure must be captured entirely, therefore triggering is important. It is important that the whole impulse signal is captured in the sampling window. By capturing the signals prior to the occurrence of the impulse, the capturing of the entire signal can be assured. The sampling of data before the trigger point is called a pre-trigger delay. The trigger is set to a certain percentage of the peak value of the impulse. By determining the sign of the voltage of the impulse, the choice of the percentage and flank for the trigger can be made.

3.3.3 Windows

For the impact testing two time domain windows are used, the force and exponential window. These windows are applied to the time signals after they are sampled, but before the FFT is calculated.

The force window is used to remove the noise present in the impulse signal. After the hammer impulse the force transducer can give a measurement signal due to noise, swinging of the hammer, placing it on a surface, etc. These 'additional forces' are not exerted on the structure. By multiplying the excitation signal with a rectangular window, these effects can be eliminated. The force window has a value of one around and during the impulse-period and is zero everywhere else. The width of the window is specified in Siglab by the force window size. The double hit amplitude is defined as a percentage of the amplitude of the first impulse. Additional impulses with an amplitude greater than this are rejected. The double hit delay is defined as a percentage of the measurement time. Impulses that occur after the double hit delay time are also rejected. [14]

The exponential window is applied to the acceleration signal. The purpose of this exponential window is to reduce leakage in the spectrum of this signal. Because of this window the acceleration signal is forced to practically zero at the end of the sampling window. The exponential window is not necessary for heavily damped structures, when the acceleration signal had damped out at the end of the sampling window. The disadvantage of the exponential window is that it introduces artificial damping to the modes of the structure. The added damping is a known damping, so it can be subtracted during the postprocessing.

3.3.4 Averaging

Because the accuracy of the calculated FRF measurements depends for a large part on the skill of the one doing the impacting, FRF measurements should be averaged. If the various FRFs are of equal importance, the averaging can be linear. This is called additive averaging. The FRFs are measured using 5 impacts at the same location per measurement.

Overlap for the averaging can only be used when the measurements are mutually uncorrelated, this is not the case for impulse signals, so no overlap can be used.

With the double hit reject the frames with more than one impulse are rejected. With an overload reject, the impacts that exceed the measurement ranges are automatically removed. [14]

3.3.5 Frequency range

The useful frequency range depends on the used tip of the hammer. This range can be determined by the auto power spectrum of the excitation signal by the following rule of thumb: the useful frequency range is determined by the frequency where the auto power spectrum of the excitation signal has a decay of 20 dB.

There exists a chance that non-linear dynamics are excited by the impulse excitation which result in low-frequent noise in the FRF.

The measurement time needed depends on the sample frequency f_s and the record length T . The distance between the spectral lines can be calculated using Eq. 3.1.

$$dF = \frac{1}{T} \quad (3.1)$$

3.3.6 Voltage range

In Siglab the voltage range and type of voltage of each channel can be specified. The type of voltage range is a bias for both channels.

The range of the channels depends on the energy applied at the system and the amount of damping present in the system. The voltage range should be as small as possible without the occurrence of an overload in one of the channels. The smaller the voltage range, the higher the voltage resolution. When the range is chosen too large, the analog to digital conversion results in a very coarse resolution, this introduces quantization noise.

3.3.7 Reproducibility

The reproducibility of the measurements can be checked by alternating measurements. When the accelerometer is placed at location 1 and the structure is excited at location 2, the resulting FRF should be the same as the measurement when the accelerometer is placed at location 2 and the excitation takes place at location 1.

3.3.8 Driving point measurements

A driving point measurement is a measurement with the accelerometer and the excitation at the same location. This measurement can be used for postprocessing purposes and to get an indication of the quality of the measurement loop.

For postprocessing purposes the driving point measurement is needed to scale the residues to Unit Modal Mass (UMM), as discussed in Section 2.3.2. The driving point measurement has no influence on mode shapes. The mass-sensitivity of a structure can be determined by this measurement. The acceleration a and applied force F are known in the same point. With the formula $F = ma$, the mass m can be determined. Using this mass, the residues can be scaled to UMM [13].

For the indication of the quality of the measurement loop, the phase of the driving point FRF is important. Between the location of excitation and the location of the response no node lines can exist, therefore no phase differences greater than 180° should occur in the phase diagram. Between every two resonances an anti-resonance should be located. A phase difference of the driving point FRF greater than 180° can indicate that the measurement loop is of bad quality.

Chapter 4

Modal analysis beam

Before performing a modal analysis on the H-drive, first a modal analysis of a simple beam structure is performed. The goal of this modal analysis is to obtain the modal parameters up to 1000 Hz. Both bending and torsional modes are desired. This chapter consists of first a description of the beam structure. Then the measurements performed on the beam are treated. Finally the postprocessing and resulting modal parameters are discussed.

4.1 The beam structure

The beam structure used for the modal analysis is a simple beam with 10 blocks screwed on top and below the main beam. A picture of the beam is shown in Fig. 4.1. A schematic reproduction together with the dimensions of the beam can be seen in Fig. 4.2. The beam is placed on either side on a piece of foam, which are glued to a stand. The beam is assumed to be free in its movements, so the stiffness and damping introduced by the foam are assumed to be negligible. Furthermore the beam is assumed to have a homogeneous mass distribution.

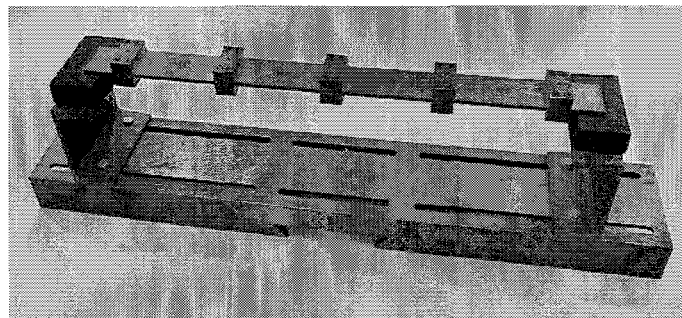


Figure 4.1: picture of the beam and support

4.2 Experiments

Before experiments can be performed, the locations of the hammer-excitation and the location of the accelerometer have to be determined. The proper tip of the hammer has to be chosen to obtain measurements up to the desired frequency. Furthermore the settings of the FFT analyzer must be adjusted. After determining the quality of the measurement loop, measurements can be performed.

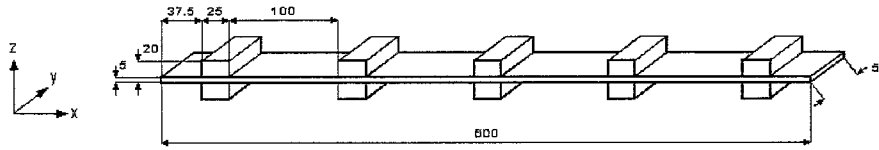


Figure 4.2: schematic reproduction beam. Dimensions in [mm].

4.2.1 Measurement points

First a measurement frame has to be chosen. The directions of the x , y and z axes of the frame can be seen in Fig. 4.2. The origin of the measurement frame is placed on top of the beam, exactly in the middle.

The goal of the modal analysis is to obtain bending and torsional modes up to 1000 Hz. Because torsional modes are desired, measurement points must be present outside the line of the heart of the beam. For visualization of modes and calculation of modal parameters in both z and y direction two modal analyses are performed.

To be sure that all modes are visible in the measured FRFs the accelerometer must be placed outside a node of a mode. Therefore the accelerometer is placed outside the line of the heart of the beam and next to the second block, at the coordinates $(x, y, z) = (-0.1, 0.0125, 0)$. For the locations of the hammer excitation the beam structure is divided into a grid of points. On the line of the heart of the beam 9 points are chosen, five on top in the center of each block and four in the middle between two blocks. Furthermore measurement points are placed on top, on the corners of each block. This results in a total of 29 excitation points. The location of the accelerometer has label 39 and the excitation points are labelled 1 up to 29.

For the y -direction the accelerometer is placed on the side of the beam-structure, outside the middle of the beam, at the coordinates $(x, y, z) = (-0.1, 0.05, 0)$. On the other side of the beam the excitation points are placed. The excitation points are placed at the same x -coordinates as the points on the line of the heart for the measurements in z -direction. The location of the accelerometer in y -direction is labelled 40 and the nine excitation points have labels 30 up to 38.

The coordinates of the points with respect to the measurement axes can be found in Appendix A.

4.2.2 Hammer tip

As explained in Section 3.3.5, the used tip of the hammer determines the useful frequency range. The maximum frequency of interest is 1000 Hz, therefore a hammer tip has to be chosen which has a decay less than 20 dB up to 1000 Hz. The auto power spectrum of an excitation signal with a hammer with teflon tip on the beam structure is shown in Fig. 4.3. In this figure can be seen that the auto power spectrum has a decay of 20 dB at approximately 1280 Hz. Since the maximum frequency of interest is 1000 Hz the teflon tip can be used for the experiments. To be sure that the force is exerted at one point and not at a surface the tip has to have a round shaped tip.

4.2.3 Settings FRF analyzer

The settings of the FRF analyzer determine the quality of the measurements considerably. More information about the settings can be found in [14].

The minimal voltage ranges are determined experimentally by decreasing the voltage ranges during several measurements and detecting the first voltage range where an overload occurs. The voltage range above this is the minimal voltage range. For the beam structure, the voltage range

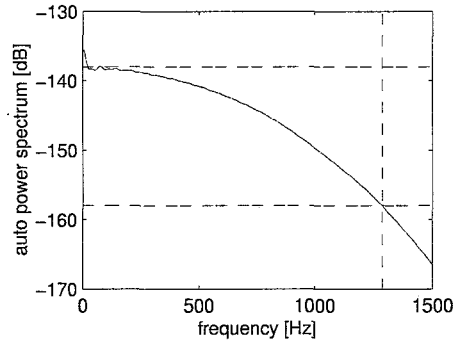


Figure 4.3: auto power spectrum excitation signal

of the hammer is set to 0.63 V and the voltage range of the accelerometer to 5 V.

The spectral resolution used for the measurements is 1.25 Hz. Frames with double hits are rejected and no overlap is used.

The signals are measured using triggering, the excitation signal is triggered at a slope of 35% on a positive flank, and a pre trigger delay of -2.3 % is used to ensure that the whole impulse is captured.

Because the beam structure is a weakly damped system modal windows have to be used. The values of the parameters determining the windows are the same as for the calibration experiments and can be found in Table 3.3. More information of the various settings and their effect can be found in Section 3.3 and in [14].

4.2.4 Driving point measurements

The quality of the measurement loop is tested using a driving point measurement. This measurement is used in the postprocessing for determination of the modal masses, as explained in Section 3.3.8.

Fig. 4.4 shows the FRF of the driving point measurement in z-direction. For this measurement the accelerometer is placed at point 39 in z direction and the force is applied at the bottom of the beam at point 39 in -z direction.

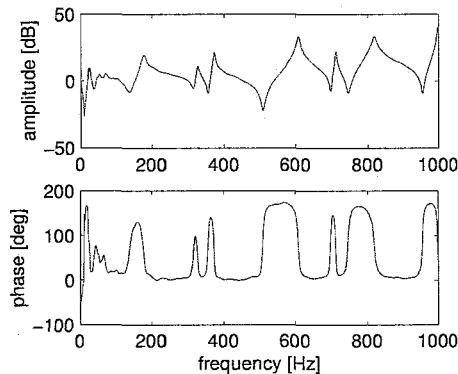


Figure 4.4: driving point z direction

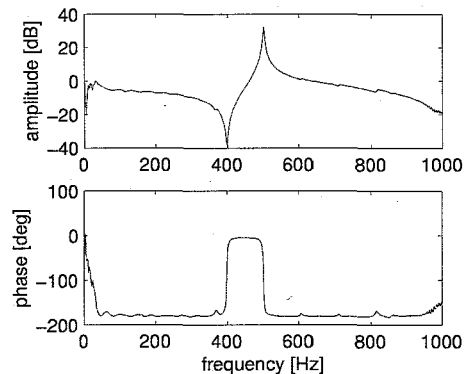


Figure 4.5: driving point y direction

The phase of the driving point measurement of Fig. 4.4 has no differences greater than 180° . For low frequencies the phase is less than zero, this results in a difference in phase greater as 180° for low frequencies and could indicate a bad measurement loop. However the low frequent difference is caused by the quality of the sensor and is not an indication of a bad measurement loop.

For the y-direction the driving point measurement is shown in Fig. 4.5. The phase of this FRF also has no differences greater than 180° , disregarding the low frequencies, so the quality of the measurements in y-direction seems also all right.

4.2.5 Reproducibility

An other indication about the quality of the measurements is to check the reproducibility. This can be done in two ways. First by determining the same FRF with the accelerometer and the hammer at the same points for a number of times. Second by interchanging the locations of excitation and response. This section deals with the second type of measurements. Fig. 4.6 shows the FRF of the measurement with the accelerometer at point 4 and the hammer excitation at point 6 and the measurement with the accelerometer at point 6 and the hammer excitation at point 4. The FRFs match perfectly, there is only a small difference between the two FRFs at the anti-resonance between 800 Hz and 1000 Hz.

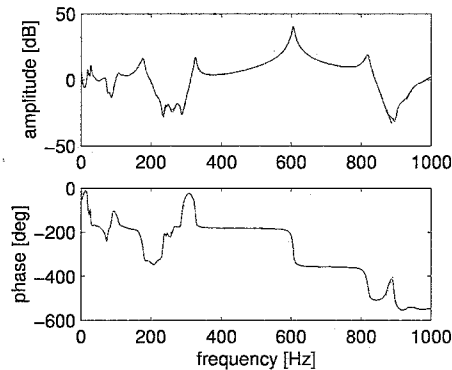


Figure 4.6: reproducibility: H_{64} (solid), H_{46} (dashed)

The small differences between the two FRFs can be ascribed to the small differences in measurement locations. The measurement location with the accelerometer at a certain point and the measurement location with the hammer at the same point do not exactly match. This causes small differences in the FRFs. An other reason is the introduction of an extra mass by the accelerometer. This extra mass is placed at different points for both measurements, this can also cause differences in the measured FRFs. Both sources of errors are of more influence when two points are chosen from which one point is outside the line of the heart of the beam.

4.2.6 Modal measurements

The FRF between each set of acceleration and excitation point can be measured using the measurement points, the tip and the settings described before. The measurement channels are labelled with the number of the location and the direction of the measurement, for example for the z measurements the channel label of the acceleration signal is 39z.

The amplitude for the measured FRFs for the z direction are shown in one graph in Fig. 4.7. This figure shows several peaks, which are resonance frequencies of the beam. The frequencies of the resonances are the same for each measurement, but the amplitude differs. The resonance frequencies of the measured FRFs do not coincide for frequencies up to 150 Hz, the measurements are of bad quality up to this frequency. Explanations for the shift in frequency are a small movement of the beam on the foam, or a not small enough spectral line spacing. With this measurements the resonances from a frequency of 150 Hz are fitted. To obtain the resonances at lower frequencies new measurements have to be performed without the use of the modal window and with a greater spectral density. This lies outside the goal of this report.

For the y direction the amplitude of the measured FRFs is shown in Fig. 4.8. The resonance

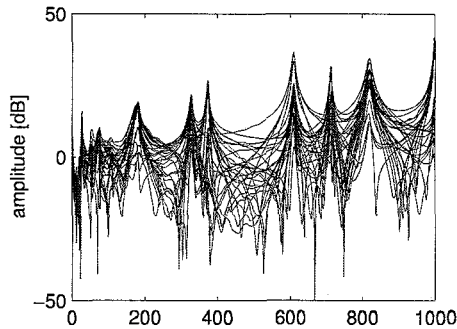


Figure 4.7: amplitude measured FRFs z direction

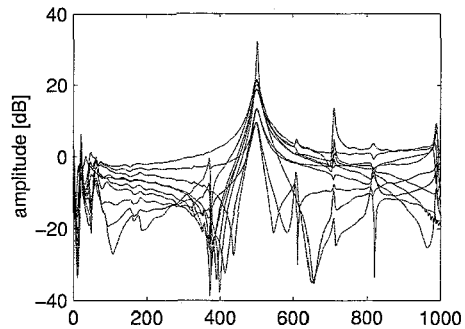


Figure 4.8: amplitude measured FRFs y direction

frequencies of these measurements do not coincide for frequencies up to 150 Hz, so again only resonances above 150 Hz are taken into account. The figure shows one great resonance peak above 150 Hz and two small ones before and after the main one. These small ones are exactly at the same frequency as resonance peaks appearing in the z measurements. These resonance peaks are not pure modes in y direction but modes with components in both y and z direction as will turn out in Section 4.3.

4.3 Results

Using ME'scope the measured FRFs can be fitted to obtain the modal parameters. The fitting is performed using the Global Polynomial method, discussed in Section 2.3. When the fit in the specified cursor band is not the same as the measured FRFs, more extra numerator polynomial terms can be used. These extra numerator polynomial terms compensate for the influence of other out-of-band modes. If increasing the extra numerator polynomial terms does not improve the fit, the number of modes that is fitted in the cursor band can be increased to improve the fit.

To visualize the mode shapes a structure has to be made in ME'scope. [13] This structure contains the measurement points and the outline of the beam structure. The measurement points are numbered in the same way as during the measurements. The measurement data can be linked to the points in the structure by matching the numbers. Lines are drawn between the measurement points to make the mode shapes more clear. The outline of the beam structure is only to get a better notion of the different mode shapes, it will not animate.

4.3.1 Modal parameters

The resonances of the measured FRFs are fitted one at a time using the Global Polynomial method while taking all measurements into account. To get the best possible fit of each of the resonances, the number of extra numerator polynomial terms used for the fits is varied between 4 and 8. The residues are scaled to Unit Modal Mass using the driving point measurements, as explained in Section 3.3.8.

For the z direction six resonances are fitted above 150 Hz. The frequency and damping of these fitted resonances is shown in Table 4.1. The residues of each resonance with respect to each measurement point can be found in Appendix B. These residues are scaled to UMM.

For the y direction only one resonance is fitted above 150 Hz. The two small resonances are not fitted. From the FRFs of Fig. 4.8 it appears that only one mode exists at 500 Hz. However the resonance can not be fitted properly using only one mode, regardless of the number of extra numerator polynomial terms. The resonance can only be fitted correctly using two modes. The frequencies and damping of these fitted modes is shown in Table 4.2. The residues of these fitted modes can again be found in Appendix B.

<i>Shape</i>	<i>Frequency [Hz]</i>	<i>Damping [%]</i>
1	177	3.06
2	326	0.970
3	372	0.646
4	608	0.586
5	711	0.283
6	818	0.734

Table 4.1: frequency and damping resonances z direction

<i>Shape</i>	<i>Frequency [Hz]</i>	<i>Damping [%]</i>
1	500	1.65
2	502	0.293

Table 4.2: frequency and damping resonances y direction

4.3.2 Mode shapes

With the fitted modal parameters, the mode shapes can be displayed by matching the measurement points to the points of the structure. The mode shapes are displayed using auto scaling. With auto scaling each shape is scaled relative to its own maximum shape component. This is done to better visualize the modes. When the modes are displayed with relative scale, the modes are scaled relative to the maximum magnitude of all shape values in the connected shape table. With relative scaling the shapes are less visible. The disadvantage of auto scaling is that small errors in measurement points are increased.

A three dimensional view of the shapes in z direction can be seen in the Figures 4.9 up to 4.14. The thick lines indicate the mode shape. A quad view of these modes, containing the three dimensional view together with a front, top and right view can be found in Appendix C.

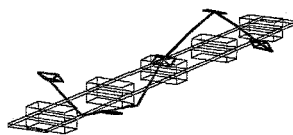
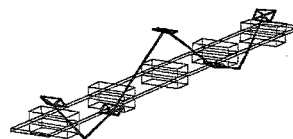
Figure 4.9: 2nd bending mode in z direction at 177 HzFigure 4.10: 3rd bending mode in z direction at 326 Hz

Fig. 4.9 shows the mode shape of the resonance at 177 Hz, this is the second bending mode of the beam in z-direction. The first bending mode, together with the rigid body modes, lie below 150 Hz and are not fitted. The third bending mode can be found at 326 Hz and is displayed in Fig. 4.10. In Fig. 4.11 the first torsional mode is shown. This mode also has a component in y direction. This is why the small resonance at 326 Hz appears in the y measurements. The fourth fitted mode is the fourth bending mode in z direction, this mode can be seen in Fig. 4.12. The second torsional mode is displayed in Fig. 4.13. This mode also has a component in y direction and again a small resonance at 711 Hz appears in the y measurements. The last shape for the z

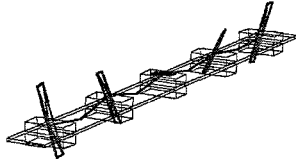


Figure 4.11: 1st torsional mode in z direction at 372 Hz

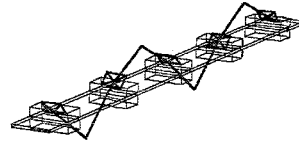


Figure 4.12: 4th bending mode in z direction at 608 Hz

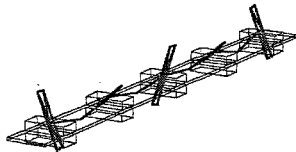


Figure 4.13: 2nd torsional mode in z direction at 711 Hz

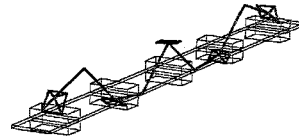


Figure 4.14: 5th bending mode in z direction at 818 Hz

direction is the fifth bending mode and lies at 818 Hz, this mode is shown in Fig. 4.14. So all six modes in z direction have a clear mode shape which would be expected. The torsional modes have both a component in y and z direction. This is why resonances appear in both the FRFs from the z and y measurements at the frequencies of the torsional modes.

For the y direction the three dimensional mode shapes are displayed in the Figures 4.15 and 4.16. A quad view of these modes can be found in Appendix C.

The mode at 500 Hz is the first bending mode of the beam in y direction, as can be seen in Fig. 4.15. The resonance below 150 Hz is the rigid body mode of the beam in y direction, but this resonance is not fitted because of the reasons stated before. The second mode at 502 Hz can be seen in Fig. 4.16. It appears to be folded around the middle. As will be seen in Section 4.3.3 the two modes are really two separate modes. The reason that the mode is not straightly bend is that there are small measurement errors and these errors are blown up by the auto scaling.

4.3.3 MAC values

The modes can be compared using the MAC values as discussed in Section 2.3.2. For the modes in z direction, the MAC values can be found in Table 4.3. On the diagonal of this table all MAC values are 1, the MAC value between the same modes is 1 because the modes are identical. All other MAC values are between 0 and 0.9, so the modes are all different.

Table 4.4 contains the MAC values of the two modes in y direction. The MAC value between the two modes is $0.002 < 0.9$. This indicates that the two modes are different and the resonance

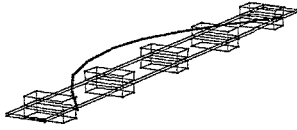


Figure 4.15: 1st bending mode in y direction at 500 Hz

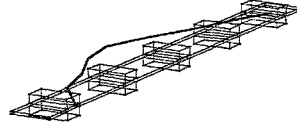


Figure 4.16: folding mode in y direction at 502 Hz

	<i>Shape 1</i>	<i>Shape 2</i>	<i>Shape 3</i>	<i>Shape 4</i>	<i>Shape 5</i>	<i>Shape 6</i>
<i>Shape 1</i>	1	0.001	0.002	0.072	0.001	0.016
<i>Shape 2</i>	0.001	1	0.000	0.003	0.001	0.193
<i>Shape 3</i>	0.002	0.000	1	0.002	0.000	0.003
<i>Shape 4</i>	0.072	0.003	0.002	1	0.002	0.009
<i>Shape 5</i>	0.001	0.001	0.000	0.002	1	0.003
<i>Shape 6</i>	0.016	0.193	0.003	0.009	0.003	1

Table 4.3: MAC values modes z direction

in y direction is caused by two closely spaced modes.

	<i>Shape 1</i>	<i>Shape 2</i>
<i>Shape 1</i>	1	0.002
<i>Shape 2</i>	0.002	1

Table 4.4: MAC values modes y direction

Chapter 5

Modal analysis H-drive

After performing a modal analysis on a beam structure as described in Chapter 4, the structure of interest, the H-drive, can be taken under consideration. This chapter first gives an description of the H-drive. As base for the modal analysis servo measurements are performed. The resulting FRF will be the FRF to which the modal data are compared. Then the modal experiments, together with the experimental aspects and the comparison between modal and servo measurements will be discussed. Finally this chapter deals with the postprocessing of the modal measurement and the obtained modal frequencies, modal damping and mode shapes.

5.1 The H-drive

The system under consideration is designed by Philips and is used for mounting IC's [11]. The system uses three linear motors, placed in the shape of an H. Therefore the system is called an H-drive.

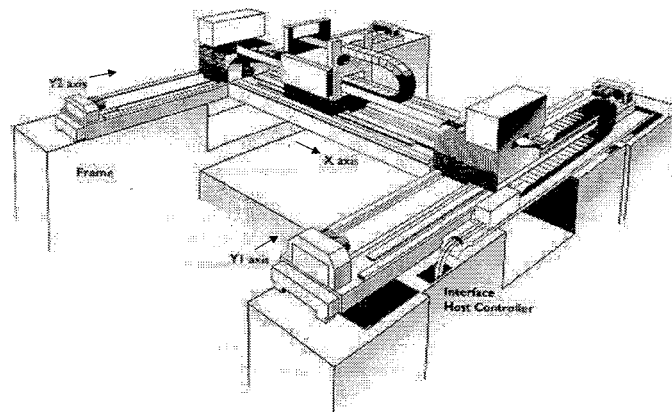


Figure 5.1: the H-drive

Fig. 5.1 shows the two parallel moving y motors, which together drive a beam on which the x drive is located. The x slide carries the placement head. A problem of H-drive manipulators is the kinematic over constraining of the x beam suspension. This is resolved by a flexure based kinematic support enabling high drive stiffness. A comparable approach is applied for the connection between base frame and y beams, since relative expansion might cause the y beams to bend. The positive directions of both y beams and the x beam is depicted in Fig. 5.1. Since an orthogonal righthanded axes frame is used this results in a z direction pointing upward. The origin of the frame is placed at the front of the y axis and the right of the x axis. If the head moves to the left, it moves in

negative x direction. If the x beam moves forward it moves in positive y direction.

For further use, the different parts of the H-drive are given the following names. The beam along the y1 axis is called Y1beam and the beam along the y2 axis Y2beam. The x beam will be referred to as Xbeam. The placement head on the x beam is named Xhead. The two heads on the y1 axis and y2 axis are called respectively Y1head and Y2head.

5.2 Servo measurements

The FRF of the Xhead is measured using a so called sensitivity measurement. The system is controlled by a lead/lag controller with a small gain, such that the controlled system has a low bandwidth. Since the modal measurements are measured with the system in a certain configuration, the FRF needs to be measured in the same configuration in order to compare the measurements. The x and y positions of the Xhead are $(x, y) = (-0.27, 0.815)$. In this configuration, the Xbeam is placed between Y1beam and Y2beam exactly above a connection to the base frame. The Xhead is placed in the middle on the Xbeam.

To minimize the effect of friction during the measurements the Xhead is moved with an sinusoidal signal around the middle of the Xbeam. The sinusoidal signal has a frequency of 8 rad/s and an amplitude of 0.02 m. The reference signal is used to bring the Xhead in the desired position. Once this position is reached the sinusoidal signal is added to the reference signal. To excite the system at a wide frequency range a noise is injected to the system. The noise is assumed to approximate a white noise signal which contains all possible frequencies in the range from 0 Hz to 1000 Hz. Fig. 5.2 shows the control scheme of the x-axis. In this figure 'H' denotes the H-drive, 'C' the controller, 'u' the control input, 'y' the output, 'r' the reference, 'e' the error and 'w' the noise.

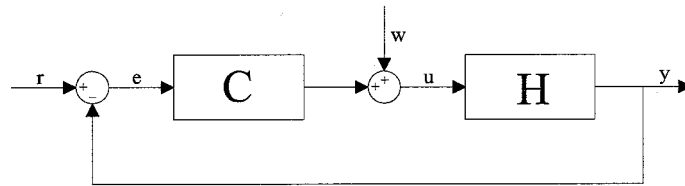


Figure 5.2: control scheme x axis

By measuring the noise 'w' and the control input 'u' the sensitivity 'S' can be computed with the following formula,

$$\frac{U}{W} = S = \frac{1}{1 + CH} \quad (5.1)$$

By dividing out the know controller 'C', the transfer function of the plant 'H' can be computed. The FRF of the plant 'H' is shown in Fig. 5.3.

The FRF of Fig. 5.3 shows overall a slope -2 and a phase of -180° . Furthermore a couple of resonances can be seen at different frequencies. From 500 Hz the resonances are no longer distinguishable, therefore no resonances greater than this frequency are taken into account. Using modal analysis the mode shapes that contribute to the resonances in the servo FRF can be found.

For control purposes the first two resonances are limiting the performance of the system. Therefore the goal of the modal analysis is mainly to find the mode shapes that cause the first two resonances.

5.3 Experiments

The modal analysis of the H-drive consists of six modal analyses. One modal analysis is performed on the Xbeam, one on the Xhead, one on both the Ybeams and one on both Yheads. Each modal

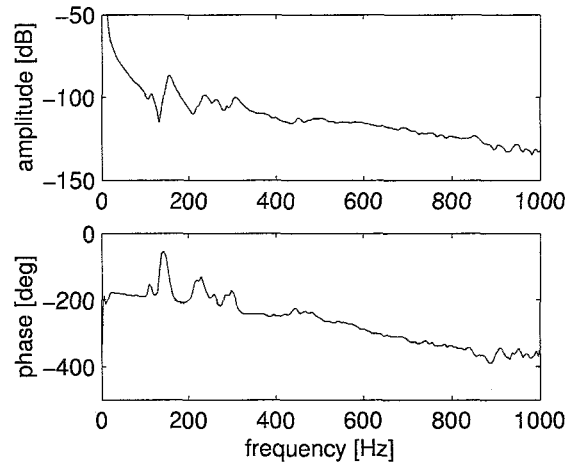


Figure 5.3: FRF H-drive servo measurement

analysis has its own measurement points, settings of the FRF analyzer, driving point measurements and reproducibility measurements. With the right settings, the modal analyses can be performed and the resulting FRFs can be compared to the FRF of the servo measurement.

5.3.1 Measurement points

For each modal analysis the measurement points have to be determined. On each part a grid of measurement points is made. The accelerometer is placed just outside the middle of the part to prevent it from being placed in a node of a mode. The points must be chosen on the main frame of the H-drive as much as possible.

On the Xbeam the measurement points for the y and z direction are placed on top of the beam, at the edges. In this way the excitation in y and z direction can be performed on the same points. This makes it possible that points can move in both y and z direction for visualizing mode shapes during the postprocessing. The points are placed 6 cm from each other. Since this grid turns out to be very fine for the frequency range of interest, not all points are used during the experiments. The accelerometer is placed on one edge of the beam, outside the middle and in z direction. For the x direction there are only two points possible, between the Xbeam and Ybeams there are only two points where the accelerometer can be placed in x direction. It is not possible to excite the Xbeam in x direction with the hammer, therefore a driving point measurement is not possible for the Xbeam in x direction.

The Xhead consists of a base and a frame mounted onto the base. The frame is less stiff and excitation on the frame is not possible. Therefore the points are all located on the base of the Xhead. The accelerometer is placed in positive x direction. The excitation points in x and y direction are chosen on the edges of the base. Because of this information can be measured in multiple directions in these points. Each edge contains three measurement points. For the z direction four points on each corner of the base are chosen.

The Ybeams are excited only in x direction, this because this direction is the direction that the servo measures. This is the only direction where modes are expected that contribute to the servo FRF. The points on each Ybeam are chosen 10 cm apart from each other. Since this grid turns out to be too fine less points are used for the modal measurements. This also reduces the measurement time. The accelerometer is placed outside the line of excitation points and outside the middle of the Ybeams.

Both Yheads are excited only in x and y direction. The accelerometer is placed in the y direction. For the x direction four points are chosen on each Head. In y direction five points are used.

The coordinates of all the excitation points and points of the accelerometer can be found in Appendix D. These coordinates use the same reference frame as used for the servo measurements.

5.3.2 Hammer tip

The tip of the hammer determines the useful frequency range, as explained in Section 3.3.5. The maximum frequency of interest is 1000 Hz. This is the same as for the beam structure. The base for the excitation is the same for both the H-drive and the beam structure. The auto power spectrum has the same shape as in Fig. 4.3. For the modal analyses of the H-drive again a teflon tip is can be used.

5.3.3 Settings FRF analyzer

The settings of the FRF analyzer for the different modal analyses are mostly the same as for the modal analysis of the beam structure and can be found in Section 4.2.3.

There is one difference. Since the H-drive is a relatively strongly damped system, no windows are used. The oscillating response signal has damped out within the time of one sampling window, so no exponential modal window is needed. Since no modal windows are used no oscillations occur in the measured FRFs.

5.3.4 Driving point measurements

To check the quality of the measurement loops of each modal analysis, driving point measurements are performed at each location of the accelerometer. These driving point measurements are also used for the scaling of the residues to unit modal mass. The FRF of the driving point measurement for the Xbeam can be seen in Fig. 5.4.

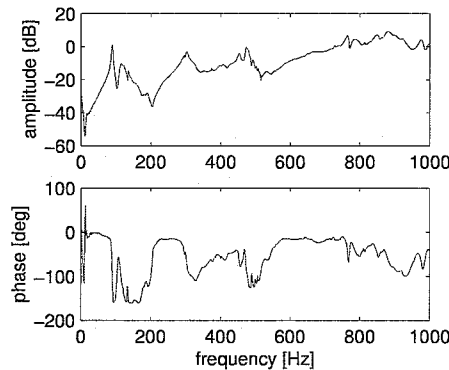


Figure 5.4: driving point Xbeam

The phase of the driving point measurement is situated between 0 and -180° . Since no leaps greater than 180° occur the measurement loop is of good quality. The driving point measurements of the other parts are comparable to the driving point measurement of the Xbeam. These measurement loops are also of good quality. The phase of the driving point measurement of the Xbeam for low frequencies is above zero. This is not an indication of a bad measurement loop, but due to the bias setting for the measurement channels. The FRF up to 0.1 Hz has to be disregarded.

5.3.5 Reproducibility

As stated in Section 4.2.5, the quality of the measurement loops can also be tested by investigation of the reproducibility of the measurements. By the reproducibility is meant the similarity between the FRFs measured with interchanging excitation and response locations.

An overlay of the set of FRFs for the Xbeam can be seen in Fig. 5.5. For the Xbeam points 12 and 31 are used. The FRFs of the Xbeam are nearly the same. The small differences are due to the not precise matching of the different points. The location of the accelerometer of the first FRF and the point of the excitation of the second FRF do not match exactly. This causes small differences in the FRFs. The reproducibility figure indicates that the measurement loop is of good quality. The reproducibility measurements of the other parts are comparable to the measurements of the Xbeam. This indicates that the other loops are also of good quality.

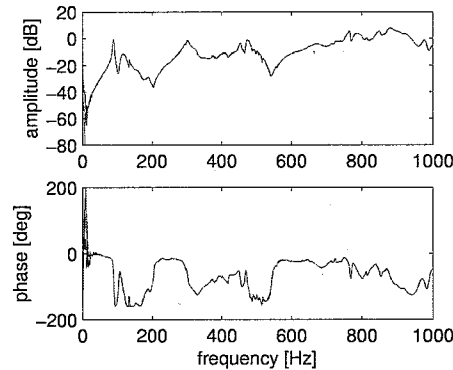


Figure 5.5: reproducibility Xbeam

5.3.6 Modal measurements

With the settings of the FRF analyzer as described in Section 5.3.3, the FRFs between each pair of excitation and acceleration points for each part can be measured.

The modal analysis of the Xbeam consists of two sets of measurements, one set for the y and z direction and one set for the x direction. For the x direction the accelerometer is placed at the two only possible points and the excitation is exerted at various points. In this way multiple FRFs can be measured, each of which provide information about the Xbeam in x direction. Because only two points are used for the x direction, the mode shapes in this direction cannot be visualized. The measured FRFs in y and z direction can be seen in Fig. 5.6. This figure shows two bands of lines, one band is for the measurements in y direction and the other for the z direction. The overlay for the FRFs of the Xbeam in x direction is shown in Fig. 5.7.

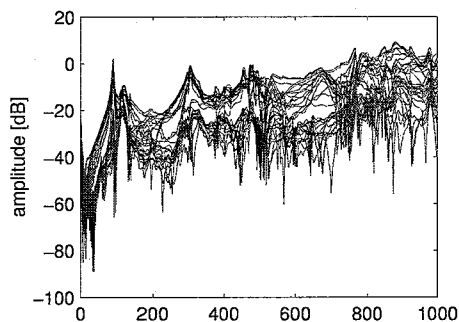


Figure 5.6: FRFs Xbeam y and z direction

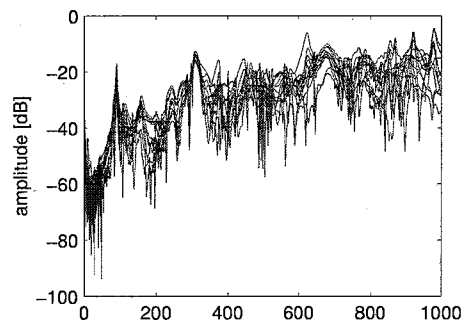


Figure 5.7: FRFs Xbeam x direction

The Xhead has excitation points in x, y and z direction. The overlaid FRFs of the Xhead show three bands of measurements, one for each direction, as can be seen in Fig. 5.8.

An overlay of the amplitude of the FRFs from the Y1beam and Y2beam is displayed in the Figures 5.9 and 5.10. The overlays of each Ybeam are very much alike, this is because the two

parts are mechanically nearly the same. There are only small differences between the Y1beam and the Y2beam in for instance the communication cables.

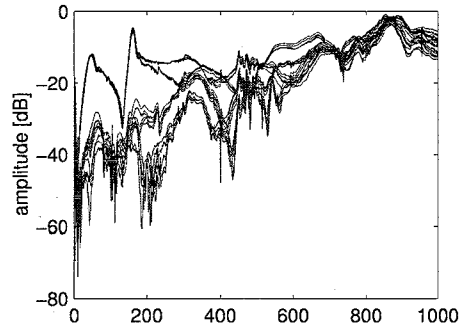


Figure 5.8: FRFs Xhead

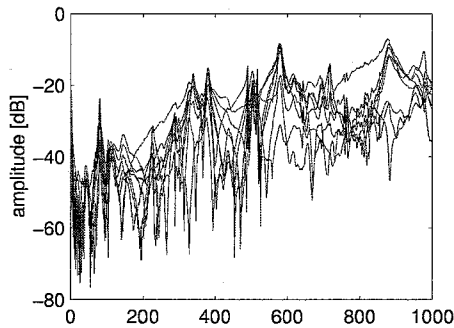


Figure 5.9: FRFs Y1beam

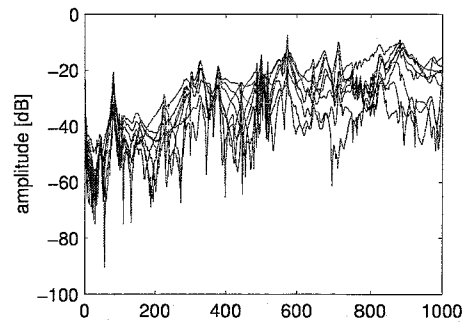


Figure 5.10: FRFs Y2beam

For the Y1head and the Y2head the amplitude of the measured FRFs is shown in the Figures 5.11 and 5.12. These figures show each two bands of measurements, one for the measurements in x direction and one for the measurements in y direction.

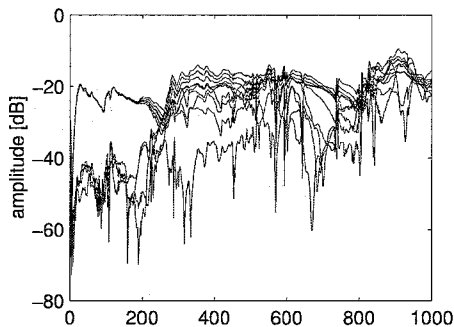


Figure 5.11: FRFs Y1head

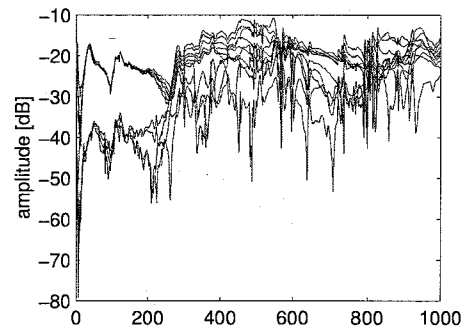


Figure 5.12: FRFs Y2head

5.4 Comparing FRFs

By comparing the FRFs of the modal measurements of each part to the servo FRF, the resonances that provoke the resonances in the servo FRF can be found. Since the resonance frequencies are

global parameters of the system, the frequencies of the resonances of the servo FRF have to match with the frequencies of the resonances in the modal FRFs. So if a resonance of a set of modal FRFs of a part matches with a resonance of the servo FRF, as far as frequency is concerned, then the resonance of the servo FRF is likely to be caused by a mode of that part. Resonances only appear in the servo FRF if energy is passed from a mode of one of the parts to the servo measurement. The servo FRF and the modal FRFs of the different parts can be found in Fig. 5.13.

The Y1beam and Y2beam show at 79.5 Hz a resonance. In the servo FRF a very small variation in the amplitude can be seen, the phase of the servo FRF shows a small bump at 79.5 Hz. This small variation is caused by the resonance in the Y1beam and the Y2beam, but this mode has only a small component in the direction of the servo measurement, the x direction, as will be seen in Section 5.5.1.

The first real resonance in the servo at 112 Hz coincides with a resonance in the FRFs of the Xbeam in both y and z direction. So a mode of the Xbeam in y and z direction provokes the resonance at 112 Hz.

The resonance in the servo FRF at 157 Hz corresponds to a resonance in the x direction of the Xbeam and to a resonance of the x direction of the Xhead. These two resonances do not have exactly the same resonance frequency. The two resonances in both parts together induce the resonance in the servo FRF at 157 Hz. These two modes are closely spaced.

A mode of the Y1beam and Y2beam at 225 Hz cause a resonance in the servo FRF to appear at the same frequency. This mode of both Y1beam and Y2beam has a clear component in the x, as will turn out in Section 5.5.1.

The fifth mode at 246 Hz is produced by a mode of the Xbeam. The FRFs of the x direction of the Xbeam show a resonance at exactly the same frequency, so the fifth resonance can be contributed to a mode in x direction of the Xbeam.

The next resonance in the servo FRF at 286 Hz is a very small one. This resonance corresponds to a very small and sharp peak in the FRFs of the Xbeam in x direction. Therefore this resonance is likely to be caused by a mode of the Xbeam in x direction. Because of the sharpness of the peak it is possible that it is caused by a signal artifact and that it is not a mode of the Xbeam. Because only two points in x direction of the Xbeam are possible, the mode shape can not be visualized to ensure that it is a mode of the Xbeam.

The resonance of the servo FRF at 305 Hz coincides with a resonance at the same frequency of the Xbeam in x, y and z direction. This resonance is therefore attributed to a mode of the Xbeam.

The last distinguishable resonance is the resonance at 452 Hz. The resonance is due to a vibration of the Xhead in x and y direction.

The resonances of the servo FRF are ascribed to resonances of the different parts by comparing the FRFs of the servo measurements and the modal measurements. Table 5.1 gives a resume of the different resonances and the parts of which modes cause them to appear in the servo FRF. In the next section a fit will be made of the resonances of interest in the modal FRFs and the modal parameters of these modes will be obtained.

<i>Frequency [Hz]</i>	<i>Unit</i>	<i>Frequency [Hz]</i>	<i>Unit</i>	<i>Frequency [Hz]</i>	<i>Unit</i>
79.5	Ybeam	159	Xhead	286	Xbeam
112	Xbeam	225	Ybeam	305	Xbeam
157	Xbeam	246	Xbeam	452	Xhead

Table 5.1: part in vibration for resonance frequencies of the servo FRF

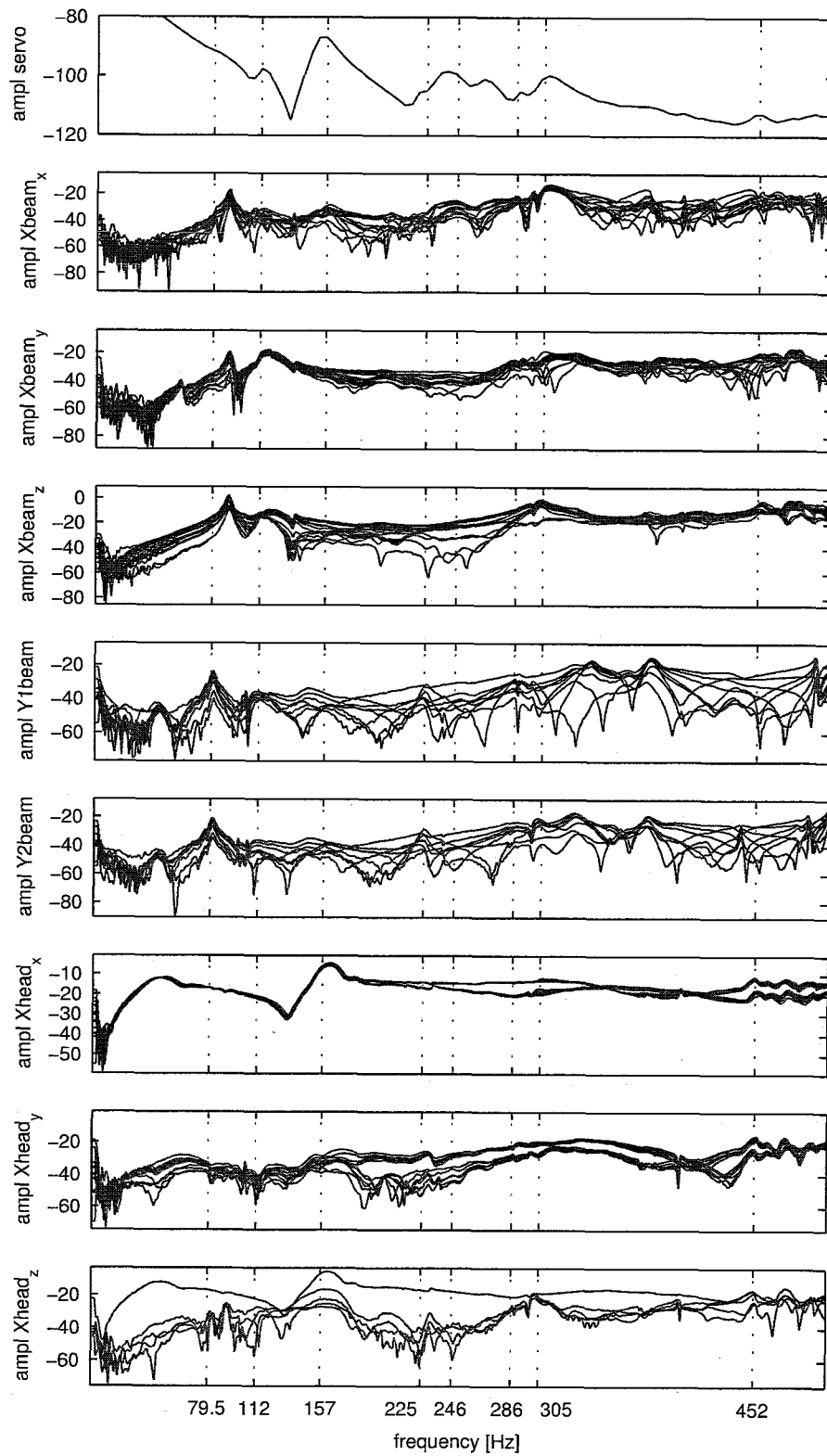


Figure 5.13: comparison of the servo FRF and the modal FRFs of the different parts

5.5 Results

The parts that induce the various resonances of the servo FRF are determined in the previous section. Now the concerned resonances of the modal FRFs of the various parts can be fitted to obtain the modal frequency, damping and the mode shape of each resonance. For the fits, the Global Polynomial method explained in Section 2.3 is used in ME'scope. The modes are fitted using the optimal number of extra numerator polynomial terms varied between 4 and 8 to obtain the best possible fits. The resulting residues are scaled to Unit Modal Mass using the driving point measurements, except the residues of the Xbeam in x direction, these are not scaled to UMM since no driving point measurement can be performed in this direction.

Table 5.2 contains the modal frequencies and damping of all the fitted modes for the various parts. The fits of the modes of the Ybeams are shown as two different shapes, this because the fits are performed on two separate data sets. The resulting modal frequencies of modes 1a and 1b are however nearly the same, the small difference can be disregarded. The frequencies of modes 5a and 5b are exactly the same, so these are also the same modes for both the Y1beam and Y2beam. The fitted damping is also of the same order of magnitude for the modes of the Y1beam and Y2beam. Shape 3 and 4 have frequencies that are closely spaced, together they provoke the second resonance of the servo FRF. The shape at 305 Hz is fitted at 301 Hz, the frequency of 305 Hz is determined visually, the real peak value is determined more accurately by the fit. The residues of these fitted modes can be found in Appendix F.

<i>Shape</i>	<i>Frequency [Hz]</i>	<i>Damping [%]</i>
1a	79.5	1.99
1b	79.6	1.84
2	112	3.82
3	157	3.17
4	159	5.21
5a	225	1.44
5b	225	1.38
6	246	2.67
7	286	0.372
8	301	0.518
9	452	0.555

Table 5.2: frequency and damping resonances H-drive

5.5.1 Mode shapes

For the visualization of the different mode shapes, the measurement points of Appendix D are added to a structure file in ME'scope. [13] An outline of the different parts of the H-drive is also added to this structure file in order to be able to interpret the mode shapes easier. For visualization purposes lines are drawn between measurement points of the various parts.

The mode shapes are visualized using auto scaling, each shape is scaled relative to its own maximum shape component, therefore small errors in measurements and in the fits result in large errors in the visualization. If relative scaling is used these errors are less significant. With relative scaling the modes are scaled relative to the maximum magnitude of all shape values in the connected shape table. The mode shapes are then less easy to interpret because of the small movements in the visualization.

3D views of the different mode shapes are shown in Figures 5.14 up to 5.19. The thick lines indicate the mode shapes. Since for the x direction of the Xbeam only two points are available, these modes can not be visualized. A quad view of the mode shapes can be found in Appendix G. The quad view contains besides the 3D view a front, top and right view.

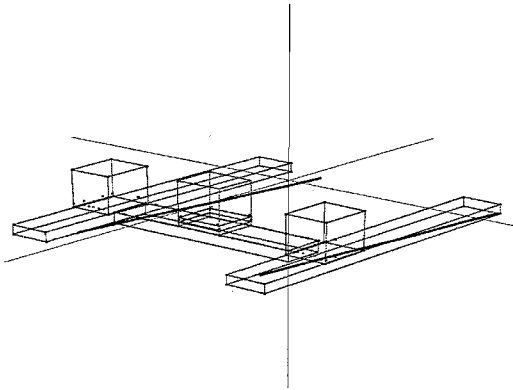


Figure 5.14: one line with one end fixed mode of the Ybeam at 79.5 Hz

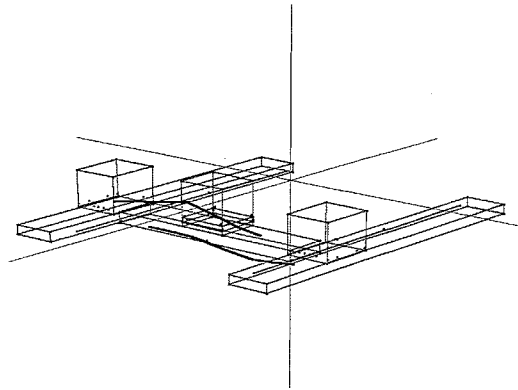


Figure 5.15: swinging mode of the Xbeam at 112 Hz

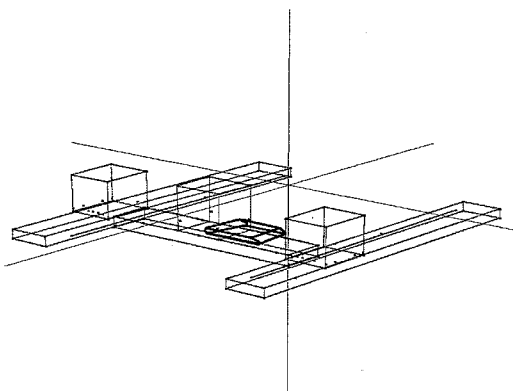


Figure 5.16: translational mode of the Xhead at 159 Hz

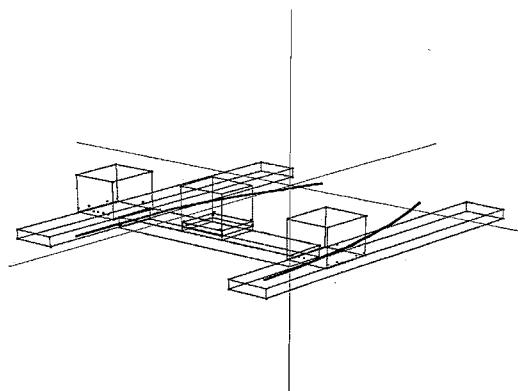


Figure 5.17: curved line mode of the Ybeam at 225 Hz

The mode of Fig. 5.14 is a mode at 79.5 Hz of the Ybeams. The Ybeams vibrate in one line with one end of the line fixed. The Xbeam is likely to connect the Y1beam and Y2beam and translates in between the two Ybeams. This mode can be caused by a weak point in the fixation of one of the Ybeams to the base frame. The Xbeam works as a stiff connection between the two Ybeams and can pass the mode to the other Ybeam. It is also possible that the fixation of both Ybeams is weak. Since the Xbeam translates as a whole for this mode, it is not likely to appear in the servo FRF. It can only appear if the Xhead moves different with respect to the movement of the Xbeam, so if the Xhead is released of the Xbeam.

The first essential mode at 112 Hz is a mode of the Xbeam. At this frequency the Xbeam swings in y and z direction and is shown in Fig. 5.15. A clear resonance peak can be seen in the modal measurements of the y and z direction and not in the x direction. This mode also shows a small bending component in y direction, this can be best seen in Fig. G.2 of Appendix C. The cause of this mode can be the non-stiff hanging of the Xbeam between the Ybeams. Two points in Fig. 5.15 do not fall in the same path as the other points. These points are located exactly in the middle of the Xhead. Since it is difficult to excite the Xbeam at these points in z direction small errors occur. Because of the auto scaling these errors are enlarged and become more visible.

The resonance caused by the Xbeam in x direction at 157 Hz can not be visualized because only two points in x direction exist, but it can be noted that the points move in phase with each other.

The fourth mode is a mode of the Xhead. The Xhead translates in x direction over the Xbeam as can be seen in Fig. 5.16. The mode also shows a difference in magnitude of the different points

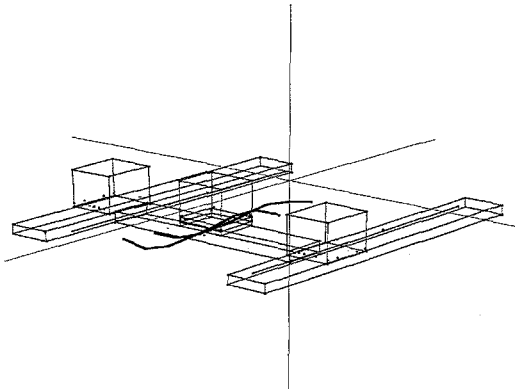


Figure 5.18: 2nd bending mode of the Xbeam at 301 Hz

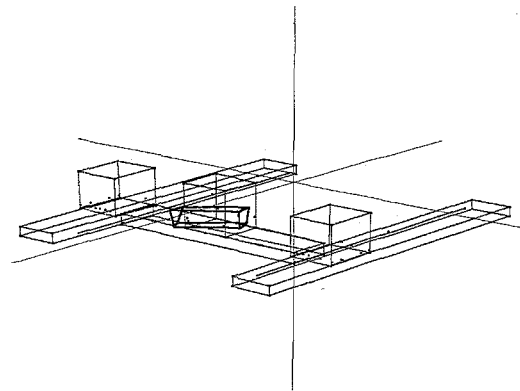


Figure 5.19: turning mode of the Xhead at 452 Hz

in x direction, the points at the bottom of the Xhead have a greater amplitude than the points at the top. This mode is not a rigid body mode, but is caused by the lower stiffness of the bearings in x direction.

The mode at 225 Hz is again a mode of the two Ybeams, shown in Fig. 5.17. Now the points on the Ybeam do not stay in one line but they form a curved line. Furthermore the two Ybeams have a phase difference of 180°, such that the Ybeams are resonating against each other. This mode will become better visible in the servo FRF since the Xbeam doesn't translate as a whole, but is suppressed by the two Ybeams.

The next two modes are both modes of the Xbeam in x direction and no visualization is possible for both modes. For both modes the two points vibrate with the same phase with respect to each other.

At 301 Hz a resonance in the servo FRF is caused by a mode of the Xbeam in x, y and z direction. The 3D visualization of this mode can be found in Fig. 5.18. The mode is the second bending mode of the Xbeam and has components in all three directions. Because of the component in x direction the mode becomes visual in the servo FRF.

Fig. 5.19 shows the mode of the Xhead at 452 Hz. At this frequency the Xhead is turning around an imaginary z axis. The mode also shows a stretching of the Xhead and a difference in amplitude of the points, the Xhead does not turn as a rigid body. Because of the high frequency and the small resonance peak it can not be ensured that the stretching is a characteristic of the mode, but it can also be due to noise and errors in the measurements.

The most important modes of the servo FRF are visualized and related to modes of the different parts. The Modal Assurance Criterion can be evaluated to compare the different modes. This is the subject of the next section.

5.5.2 MAC values

The Modal Assurance Criterion is a measure for the similarity between two modes, as stated before in Section 2.3.2.

Table 5.3 contains the MAC values of the fitted modes of the H-drive. All MAC values outside the main diagonal are smaller than 0.9, so all modes are different.

<i>Shape</i>	<i>1a</i>	<i>1b</i>	<i>2</i>	<i>3</i>	<i>4</i>	<i>5a</i>	<i>5b</i>	<i>6</i>	<i>7</i>	<i>8</i>	<i>9</i>
<i>1a</i>	1	0.000	0.000	0.000	0.000	0.608	0.000	0.000	0.000	0.000	0.000
<i>1b</i>	0.000	1	0.000	0.000	0.000	0.000	0.651	0.000	0.000	0.000	0.000
<i>2</i>	0.000	0.000	1	0.000	0.000	0.000	0.000	0.000	0.000	0.015	0.000
<i>3</i>	0.000	0.000	0.000	1	0.000	0.000	0.000	0.657	0.795	0.000	0.000
<i>4</i>	0.000	0.000	0.000	0.000	1	0.000	0.000	0.000	0.000	0.000	0.330
<i>5a</i>	0.608	0.000	0.000	0.000	0.000	1	0.000	0.000	0.000	0.000	0.000
<i>5b</i>	0.000	0.651	0.000	0.000	0.000	0.000	1	0.000	0.000	0.000	0.000
<i>6</i>	0.000	0.000	0.000	0.657	0.000	0.000	0.000	1	0.705	0.000	0.000
<i>7</i>	0.000	0.000	0.000	0.795	0.000	0.000	0.000	0.705	1	0.000	0.000
<i>8</i>	0.000	0.000	0.015	0.000	0.000	0.000	0.000	0.000	0.000	1	0.000
<i>9</i>	0.000	0.000	0.000	0.000	0.330	0.000	0.000	0.000	0.000	0.000	1

Table 5.3: MAC values modes H-drive

Chapter 6

Position dependency

The resonance frequencies of the servo FRF vary with the position of the Xbeam and Xhead [12]. By changing the y position of the Xbeam and the x position of the Xhead the inertia and the stiffness of the system are altered, this results in a frequency variation of the resonances. To investigate the influence of the frequency shift of the resonances, first the servo FRFs are measured with the Xhead placed at the corners of a square. Next a configuration is chosen at which a second modal analysis is performed. The measurements and results are described after this. Finally the results of the second modal analysis are compared to the results of Chapter 5.

6.1 Servo measurements

The configuration used in Chapter 5 is used as the first position. By changing one variable, the x or the y position of the Xhead, at a time the servo FRFs can be compared. The four servo FRFs are measured where the positions of the Xhead at the four positions form a square. The coordinates of the Xhead for each configuration are shown in Table 6.1.

<i>Configuration</i>	<i>X coordinate</i>	<i>Y coordinate</i>
1	-0.270	0.815
2	-0.510	0.815
3	-0.270	0.515
4	-0.510	0.515

Table 6.1: coordinates of the Xhead for the various configurations

The FRFs of each configuration are measured using a sensitivity measurement, described in Section 5.2. As reference signal after reaching the right position, a sinusoidal signal is used with an amplitude of 0.02 m and a frequency of 8 rad/s. Again a noise is injected to the system to excite the system at a wide range of frequencies. The measured servo FRFs of the different configurations of the H-drive are shown in Fig. 6.1.

In the figures of the measured servo FRFs the frequency shift can clearly be seen. Some resonances shift in frequency and some resonances are visible in one FRF and not visible in another FRF.

Most modes of the modal analysis of Chapter 5 are located in the Xbeam and the Xhead. For the second modal analysis, the position of the Xhead is changed in x direction. The Xhead, and with this the Xbeam, stay at the same y location. Fig. 6.2 shows a picture of the H-drive in configuration 1 and Fig. 6.3 shows the H-drive in the second configuration.

The servo FRF of configuration 1 and the servo FRF of configuration 2 are plotted in Fig. 6.4. It can be seen that the resonance of 112 Hz of configuration 1 shifted a bit for the second configuration. Before this resonance a new resonance appears in the FRF of configuration 2

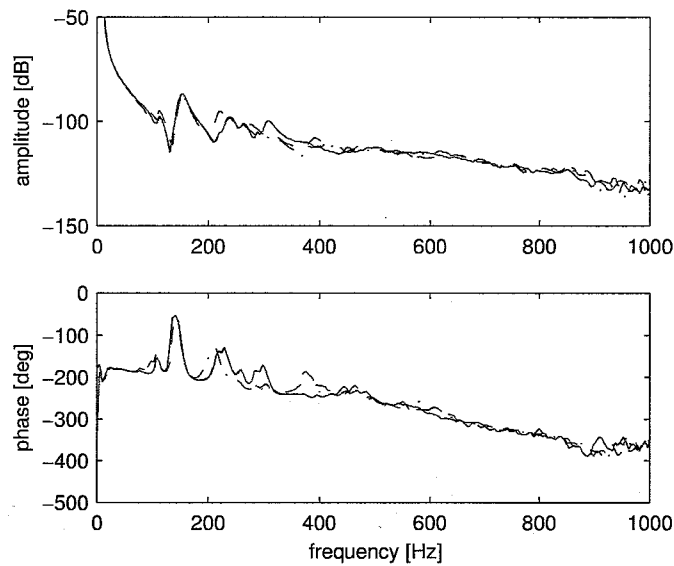


Figure 6.1: FRFs H-drive: conf. 1 (solid), conf. 2 (dashed), conf. 3 (dash-dot) and conf. 4 (dotted)

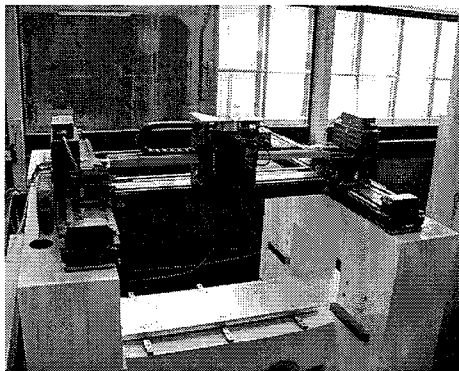


Figure 6.2: H-drive in configuration 1

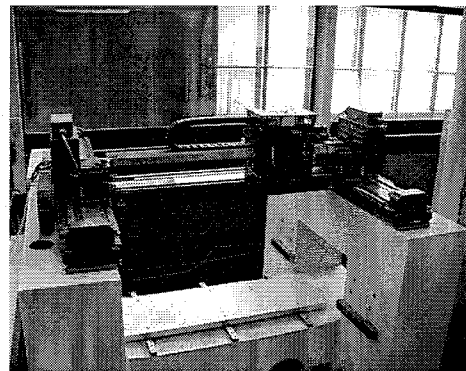


Figure 6.3: H-drive in configuration 2

which is not visible in the FRF of configuration 1. The next four resonances stay at nearly the same frequency. The fifth resonance of 286 Hz of configuration 1 shifts to a lower frequency for configuration 2. The resonance of 301 Hz of configuration 1 shifts to 277 Hz for configuration 2 as will be seen in the modal results of Section 6.3. In the region of 245 Hz up to 280 Hz the resonances are closely spaced. The resonance at 452 Hz of configuration 1 shifts to a higher frequency.

6.2 Modal experiments

The modal analysis with the system in the second configuration consists again of six separate modal analysis, one for each part of the H-drive.

The coordinates of the measurement locations are the same as for the modal analysis of configuration 1, except for the Xhead. Since the Xhead shifted 0.24 cm in the x direction, only the x coordinates of the points of the Xhead change. The new coordinates can be found in Appendix E. The used hammer tip is the same as for the modal measurements of configuration 1, a teflon tip is used. The settings of the FRF analyzer are also equal to the setting for the first configuration and can be found in Section 5.3.3.

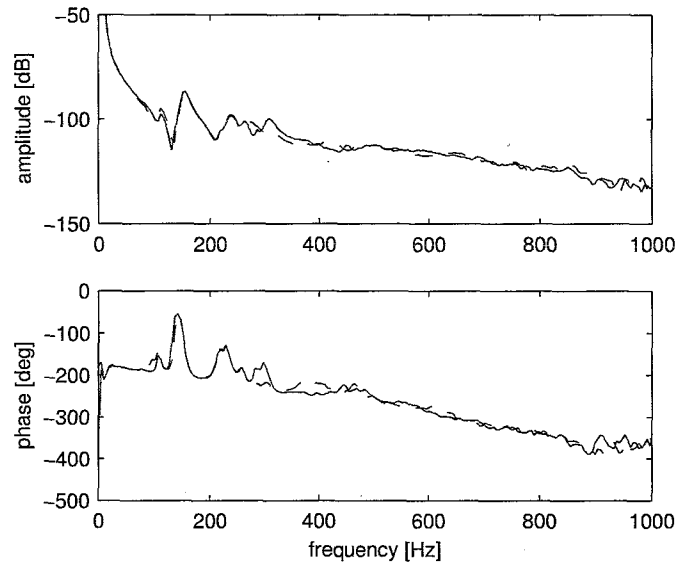


Figure 6.4: servo FRFs configuration 1 (solid) and configuration 2 (dash-dot)

For the second modal analysis new driving point measurements are performed. These driving point measurements indicate that the measurement loops for the second modal analysis are of good quality. They are also used for scaling the residues to Unit Modal Mass.

6.2.1 Modal measurements

For the second configuration modal measurements are performed on each part using the settings described in Section 5.3.3.

An overlay of the measured set of modal FRFs for the Xbeam can be seen in Fig. 6.5 for the y and z direction. Fig. 6.6 shows the modal FRFs for the x direction. Fig. 6.5 shows two bands of measurement lines, one for the measurements in y direction and one for the measurements in z direction.

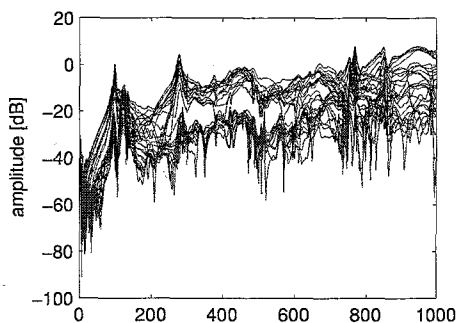


Figure 6.5: FRFs Xbeam y and z direction

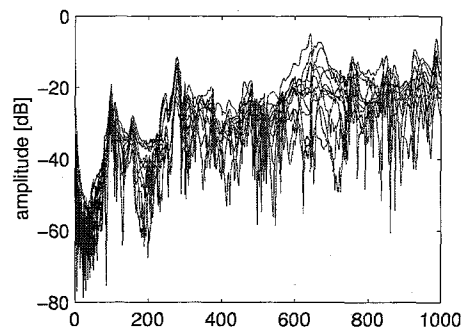


Figure 6.6: FRFs Xbeam x direction

An overlay of the FRFs of the Xhead can be seen in Fig. 6.7. Three bands are visible in this figure, one for the measurements in the x direction, one for the y and one for the z direction. The modal FRFs of the Y1beam and the Y2beam can be found in respectively Fig. 6.8 and Fig. 6.9.

Both Yheads have excitation points in x, y direction. The overlaid FRFs of the Yheads show two bands of measurements, one for each direction, as can be seen in Fig. 6.10 and Fig. 6.11.

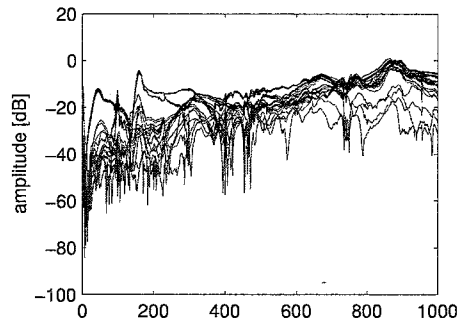


Figure 6.7: FRFs Xhead

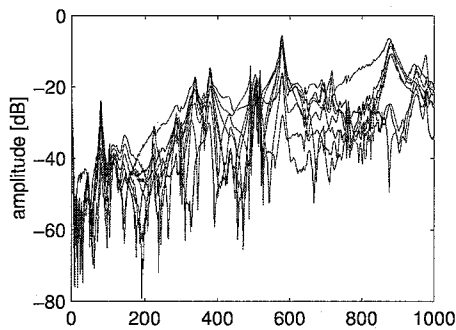


Figure 6.8: FRFs Y1beam

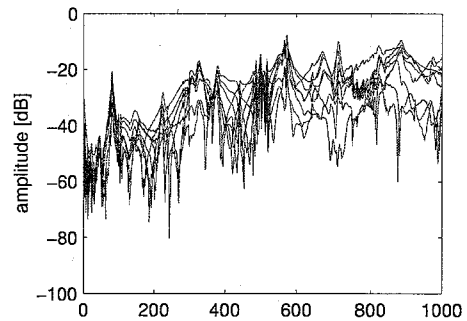


Figure 6.9: FRFs Y2beam

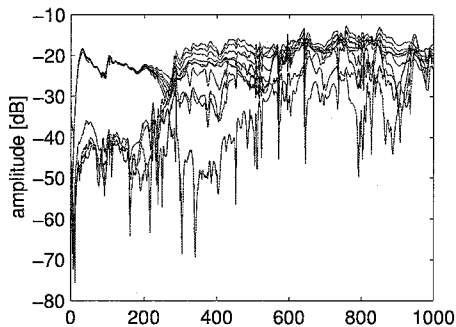


Figure 6.10: FRFs Y1head

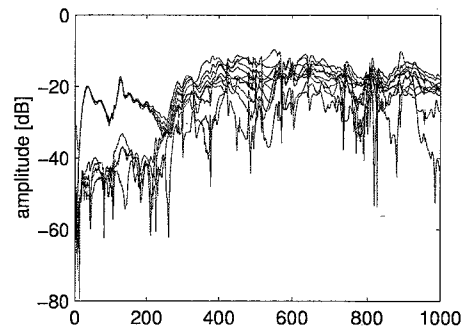


Figure 6.11: FRFs Y2head

6.2.2 Comparing FRFs

The modal FRFs of the second configuration can be compared with the servo FRF of the second configuration. The parts that cause the resonances to appear in the servo FRF can be determined by matching resonance frequencies. The servo FRF is displayed with the different modal FRFs in Fig. 6.12.

The resonance in the Ybeams at 79.4 Hz introduces a small resonance and a small phase bump in the servo FRF of the second configuration. This mode in the Ybeams only has a small contribution to the servo FRF, this will become more clear in Section 6.3.1.

The new resonance that appears at 97.8 Hz in the servo FRF can be contributed to a resonance of the Xbeam in x, y and z direction as can be seen in Fig. 6.12.

The resonance at 112 Hz is caused also by a vibration of the Xbeam, this time in y and z direction. This resonance is at the same frequency as a resonance of the first configuration and

both are caused by the same part.

The next resonance at 156 Hz is caused in the first configuration by two closely coupled resonances of the Xbeam in x direction and the Xhead. This is also the case for the second configuration.

A vibration of the Ybeams is the reason that the resonance at 224 Hz appears in the servo FRF. This resonance can also be found at nearly the same frequency in the servo FRF of configuration 1.

The next resonance is caused by a vibration of the Xbeam in the x direction.

The resonance at 277 Hz is caused also by the Xbeam, but now of a vibration in y and z direction. This resonance shifted from 301 Hz for the first configuration to this lower frequency for the second configuration. Closely spaced to this resonance, a resonance in the x direction of the Xbeam is present at 279 Hz. It could be possible that this resonance is the same resonance as the resonance of the y and z direction. The difference can be caused by measurement errors or a small difference in the position of the Xhead when the two different set of measurements are performed.

The last distinguishable resonance is the resonance at 473 Hz and is caused by a vibration of the Xhead. Compared to the first configuration this resonance shifted to a higher frequency.

Table 6.2 gives a resume of the different resonances and the parts that cause them to appear in the servo FRF. By fitting these modes the modal parameters are obtained, this will be discussed in the next section.

<i>Frequency [Hz]</i>	<i>Unit</i>	<i>Frequency [Hz]</i>	<i>Unit</i>	<i>Frequency [Hz]</i>	<i>Unit</i>
79.4	Ybeam	157	Xhead	277	Xbeam
97.8	Xbeam	224	Ybeam	279	Xbeam
112	Xbeam	244	Xbeam	473	Xhead
156	Xbeam				

Table 6.2: part in vibration for resonance frequencies of the servo FRF

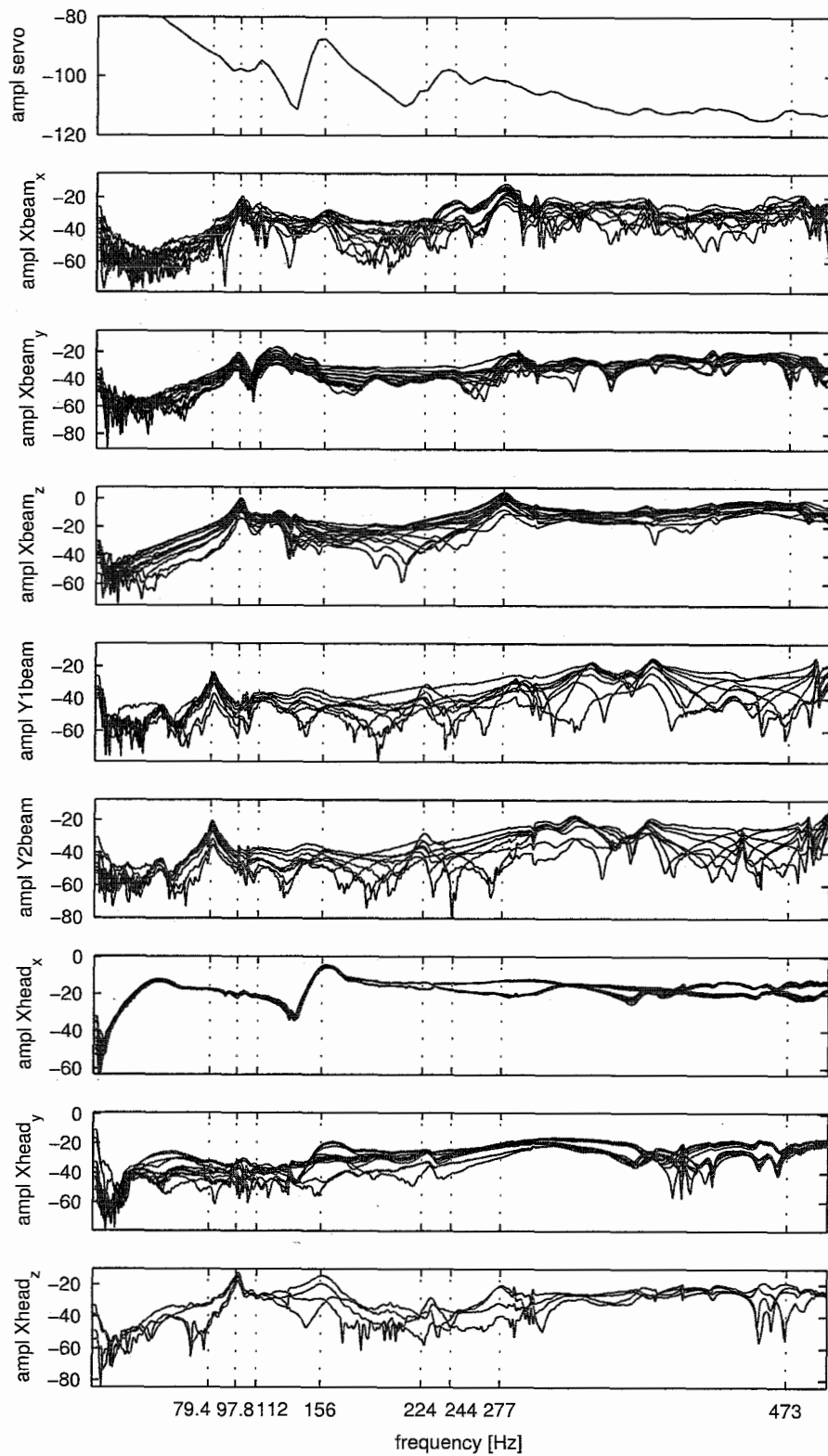


Figure 6.12: comparison of the servo FRF and the modal FRFs of the different parts

6.3 Results

The resonances described in the previous section are fitted using the Global Polynomial method. Except for the x direction of the Xbeam, the residues are scaled to UMM using the driving point measurements.

The modal frequencies and modal damping of the fitted modes can be found in Table 6.3. Note that the fitted frequency of mode 3 is not 112 Hz as expected in Section 6.2.2 but 123 Hz. An explanation for this can be that the top of the fitted resonance is quite flat in a certain frequency range. The fitted modal frequency can alternate very easy with a small change in amplitude. This small change can be introduced by for instance a measurement error. An other explanation can be that this mode is very sensitive to position. The servo FRF is measured with the Xhead moving over a range of a couple of centimeters. The servo FRF is actually an averaged FRF over a range of positions, the modal measurements are measured with the Xhead fixed at one position. This difference could be the reason for the frequency shift. Furthermore the mode of 244 Hz is fitted at 248 Hz.

The frequencies of modes 1a and 1b are nearly the same, the small difference is disregarded. The frequencies of modes 6a and 6b are exactly the same. The damping of both sets of modes are of the same order of magnitude. So modes 1a and 1b are assumed to equal, only for the two different Ybeams. Modes 6a and 6b are also assumed to be identical modes for two different Ybeams. The fitted residues can be found in Appendix H.

<i>Shape</i>	<i>Frequency [Hz]</i>	<i>Damping [%]</i>
1a	79.3	2.08
1b	79.4	2.25
2	97.8	2.34
3	123	4.55
4	156	3.58
5	157	6.00
6a	224	1.55
6b	224	1.70
7	248	1.68
8	277	2.01
9	279	1.31
10	473	1.68

Table 6.3: frequency and damping resonances H-drive

6.3.1 Mode shapes

The fitted mode shapes of Appendix H can be visualized using ME'scope. Auto scaling is used to scale the mode shapes.

The 3D views of the mode shapes of the second configuration can be found in Figures 6.13 up to 6.19. The mode shapes are displayed by the thick lines. Since for the x direction of the Xbeam only two points are available, these modes cannot be visualized. A quad view of the mode shapes can be found in Appendix I.

Fig. 6.13 shows the mode shapes of the Ybeams at 79.4 Hz. The measurement points vibrate in one line with each other, this line is fixed at one end of the Ybeams. The Xbeam translates in its entirety in between the two Ybeams and therefore this mode is not likely to appear in the servo FRF. The two Ybeams vibrate in phase with each other.

The mode at 97.8 Hz is a mode of the Xbeam and is shown in Fig. 6.14. It is the first bending mode of the Xbeam. Two points show a deviation from the rest. These two points are measurement points in the middle of the Xhead. These points are difficult to excite in the z

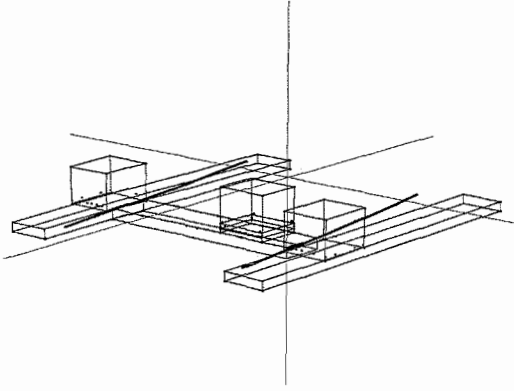


Figure 6.13: one line with one end fixed mode of the Ybeam at 79.4 Hz

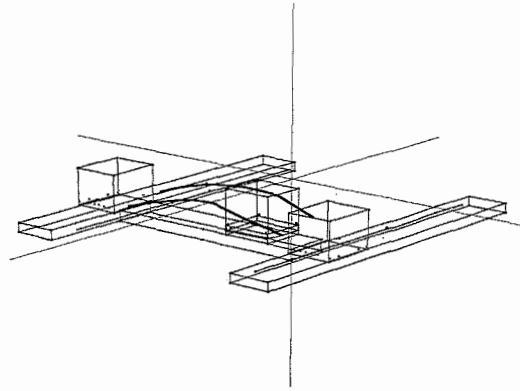


Figure 6.14: 1st bending mode of the Xbeam at 97.8 Hz

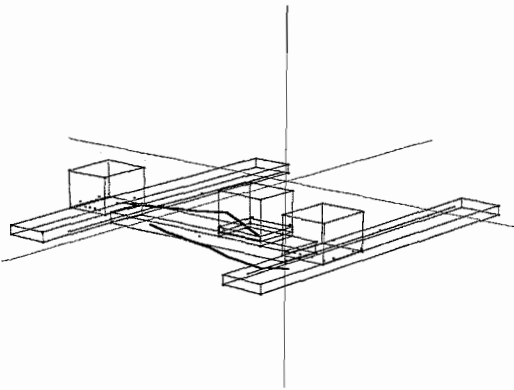


Figure 6.15: swinging mode of the Xbeam at 123 Hz

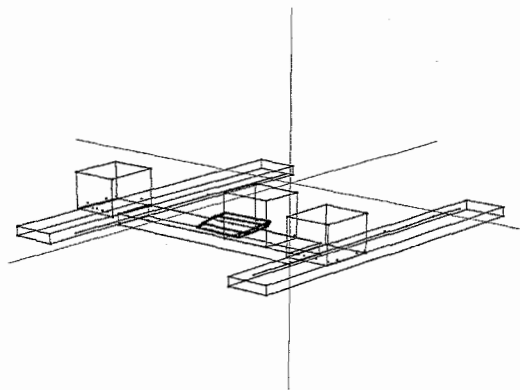


Figure 6.16: translational mode of the Xhead at 157 Hz

direction, this introduces errors in the measurements of these points in z direction. Because of the auto scaling these errors become more visible.

The third mode is fitted at 123 Hz. This mode is the swinging mode of the Xbeam as can be seen in Fig. 6.15. The two points in the middle of the Xhead show again a measurement error because of the same reason as for the previous mode. The mode also shows a difference in amplitude in y direction as can be seen in Fig. I.3 of Appendix I. The part at where the Xhead is located has a bigger amplitude in y direction as the other end of the Xbeam. This was not the case with the Xhead placed in the middle of the Xbeam for the first configuration. This change of the mode is due to the movement of the Xhead.

The mode of Fig. 6.16 at 157 Hz is the same mode as the mode of Fig. 5.16 and is located at almost the same frequency. The Xhead translates in x direction over the Xbeam. Also a difference in amplitude in x direction can be seen for points on the same edge.

The next mode that can be visualized is a mode of the Ybeams at 224 Hz and is show in Fig. 6.17. The Ybeams vibrate with the points in a curved line and in opposite phase with respect to each other.

The third mode of the Xbeam is shown in Fig. 6.18, this is the second bending mode of the Xbeam and is located at 277 Hz. This mode also had a clear component in x direction and therefore appears in the measured servo FRF.

The last mode that can be visualized is a turning mode of the Xhead. This mode is found at 473 Hz and is shown in Fig. 6.19. The mode also shows a difference in amplitude between points on the same edge, but because the mode is not as clear as the modes at lower frequencies it can

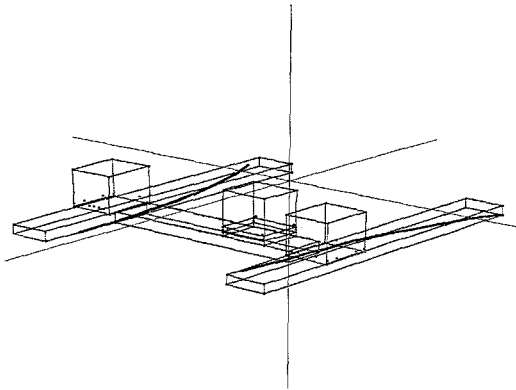


Figure 6.17: curved line mode of the Ybeam at 224 Hz

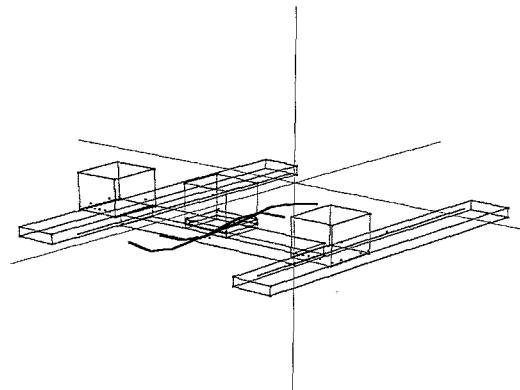


Figure 6.18: 2nd bending mode of the Xbeam at 277 Hz

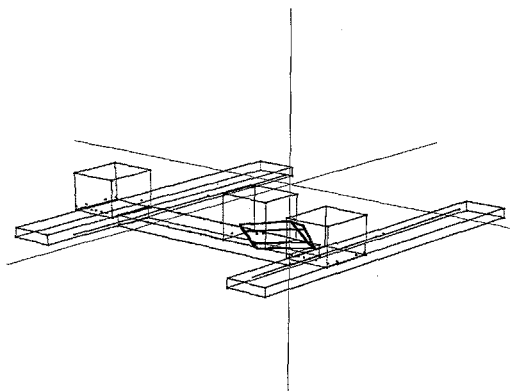


Figure 6.19: turning mode of the Xhead at 473 Hz

not be stated that this is a characteristic of the mode or that it is due to measurement errors.

In the next section the modes are evaluated using the Modal Assurance Criterion.

6.3.2 MAC values

The similarity between the various mode is evaluated using the MAC values. The MAC values for the different modes can be found in Table 6.4. Besides the ones at the main diagonal, all MAC values are smaller than 0.9 the modes are all different.

6.4 Comparing configurations

By comparing the results of the different configurations obtained in Sections 5.5 and 6.3, the influence of the change in position of the Xhead becomes visible.

Both configurations show a resonance in the Ybeams at approximately the same frequency at 79.5 Hz. The mode shapes are also the same and for both configurations the modes are nearly invisible in the servo FRFs.

In the servo FRF of the second configuration a resonance appears at 97.8 Hz which is not visible in the servo FRF of the first configuration. This resonance is caused by the first bending mode of the Xbeam. In the first configuration the Xhead is placed exactly in the middle of the Xbeam. This is the point of the first bending mode which shows no angle with the horizontal. In the middle the mode, has no component in x direction and therefore this mode is not visible in

<i>Shape</i>	<i>1a</i>	<i>1b</i>	<i>2</i>	<i>3</i>	<i>4</i>	<i>5</i>
1a	1	0.000	0.000	0.000	0.000	0.000
1b	0.000	1	0.000	0.000	0.000	0.000
2	0.000	0.000	1	0.098	0.000	0.000
3	0.000	0.000	0.098	1	0.000	0.000
4	0.000	0.000	0.000	0.000	1	0.000
5	0.000	0.000	0.000	0.000	0.000	1
6a	0.000	0.735	0.000	0.000	0.000	0.000
6b	0.655	0.000	0.000	0.000	0.000	0.000
7	0.000	0.000	0.000	0.000	0.526	0.000
8	0.000	0.000	0.226	0.045	0.000	0.000
9	0.000	0.000	0.000	0.000	0.686	0.000
10	0.000	0.000	0.000	0.000	0.000	0.324

<i>Shape</i>	<i>6a</i>	<i>6b</i>	<i>7</i>	<i>8</i>	<i>9</i>	<i>10</i>
1a	0.000	0.655	0.000	0.000	0.000	0.000
1b	0.735	0.000	0.000	0.000	0.000	0.000
2	0.000	0.000	0.000	0.226	0.000	0.000
3	0.000	0.000	0.000	0.045	0.000	0.000
4	0.000	0.000	0.526	0.000	0.686	0.000
5	0.000	0.000	0.000	0.000	0.000	0.324
6a	1	0.000	0.000	0.000	0.000	0.000
6b	0.000	1	0.000	0.000	0.000	0.000
7	0.000	0.000	1	0.000	0.786	0.000
8	0.000	0.000	0.000	1	0.000	0.000
9	0.000	0.000	0.786	0.000	1	0.000
10	0.000	0.000	0.000	0.000	0.000	1

Table 6.4: MAC values modes H-drive

the servo FRF of the first configuration. For the second configuration the mode becomes visible because the Xhead is located outside the middle and a component in x direction exists at the location of the servo measurement.

The swinging mode of the Xbeam exists in both the first configuration and the second configuration. In the servo FRFs it appears at the same frequency. For the second configuration the mode is fitted at a different frequency because of the reasons discussed in the previous section. The modes are despite of a difference in amplitude in y direction of the same nature and appear in both configurations.

The mode in the servo FRFs at 157 Hz is for both configurations caused by two closely spaced modes, a mode in the x direction of the Xbeam and a translational mode of the Xhead. The frequencies are nearly the same for both configurations, in the servo FRFs the resonances appear at the same frequency.

The second mode caused by a resonance of the Ybeams is can be found in both configurations at nearly the same frequency. The mode shapes are also the same, so the changing of the position of the Xhead does not affect the modes of the Ybeams.

The modes of the Xbeam in x direction are present in both configurations at the same frequency range. The mode at 286 Hz of the first configuration shifts to 279 Hz in the second configuration. The reason of this shift can not be explained since the mode shapes of the Xbeam in x direction can not be visualized due to the limited number of points in this direction.

The second bending mode of the Xbeam shifts from 301 Hz for the first configuration to 277 Hz for the second configuration. This shift is due to the changing inertia caused by the Xhead. By changing the position of the Xhead the inertia changes and with the changing inertia the resonance frequency changes.

The resonance caused by the turning of the Xhead is found in both configurations. In the first configuration this mode is found at 452 Hz and in the second configuration at 473 Hz. The change of the position of the Xhead also effects this mode.

Table 6.5 shows the modes of the different parts which provoke the resonances of the servo FRF for the different configurations. The resonances present in the servo FRFs are caused by the same modes of the different parts. However, the frequency of the resonances can shift with varying position of the Xhead. Some resonances, such as the first bending mode, are present in the one servo FRF and do not appear in the other. This is because of the Xhead is positioned at a location where the mode has no effect in x direction at the location of the servo measurement.

<i>Unit</i>	<i>Kind of mode</i>	<i>Freq. conf. 1 [Hz]</i>	<i>Freq. conf. 2 [Hz]</i>
Ybeams	One line with one end fixed	79.5	79.4
Xbeam	First bending mode	-	97.8
Xbeam	Swinging mode	112	123
Xbeam	X direction	157	156
Xhead	Translational mode	159	157
Ybeams	Curved line	225	224
Xbeam	X direction	246	248
Xbeam	X direction	286	279
Xbeam	Second bending mode	301	277
Xhead	Turning mode	452	473

Table 6.5: Differences between modes causing resonances in the servo FRFs for the different configurations

Chapter 7

Conclusion

Modal analysis is a measurement technique that obtains a dynamic model of a structure by retrieving the modal parameters: modal frequencies, modal damping and mode shapes. Between the roving hammer impact signal and the fixed acceleration measurement FRFs are calculated. By fitting the FRFs, the modal parameters are obtained. The fit procedure is done with the global polynomial method which is based on a least squared error fit. The quality of the measurements depends on the skills of the person doing the experiments and on the accuracy of the equipment. It also depends much on the settings of the used FRF analyzer, in this case Siglab. These settings involve triggering, windowing, averaging and adjusting the frequency and voltage ranges. The useful frequency range depends on the used hammer tip.

The data-acquisition and the calculation of the FRFs is done by Siglab. For the postprocessing of the data, such as the fitting and visualization of the mode shapes, ME'scope is used. Before performing a modal analysis on the H-drive first a servo FRF is determined using a sensitivity measurement. The servo FRF is measured with the Xhead moving around the position of interest to eliminate the influence of friction. The total modal analysis of the H-drive consists of separate modal analyses performed on each part of the H-drive. Prior to the modal experiments the measurement points of the accelerometer and the hammer impact on the several parts of the H-drive are determined. Furthermore, the used hammer tip is chosen based on the auto power spectrum of the excitation signal. The settings of Siglab are optimized for each modal analysis of the different parts to obtain the best possible results. The quality of the measurement loops are tested by performing driving point measurements. These driving point measurements can also be used for the scaling of the residues to Unit Modal Mass. The reproducibility of the measurements is also tested. With the optimal settings, FRFs are measured between each excitation signal and acceleration measurement. The modal FRFs are compared to the servo FRF to determine what resonance of which part causes the eigenmodes that appear in the servo FRF. The comparison is done by matching the resonance frequencies of the modal FRFs to the resonance frequencies of the servo FRF. This can be done since the resonance frequencies are global parameters of a system, whereas the amplitude and phase are local parameters that are different for each point. By fitting the resonances of the different parts with the global polynomial method in ME'scope, the modal parameters are obtained. The modes can be visualized with the use of a structure file in ME'scope. The mode shapes of the Xbeam in x direction cannot be visualized because the response in x direction can only be measured at two points. The resonances in the servo FRF are caused by modes of the Xbeam, Ybeams and Xhead. The first resonance that limits the performance of the controlled system is a swinging mode of the Xbeam at 112 Hz. The second limiting resonance is caused by a set of closely spaced translational modes, a mode of the Xbeam in x direction at 157 Hz and a translational mode of the Xhead at 159 Hz.

By measuring servo FRFs with the Xhead at different positions, the modal frequencies turned out to be position dependent. Since the most modes appear in the Xbeam and Xhead, the x direction of the Xhead is changed to obtain the second configuration for a new modal analysis. The resonances for the second configuration are also caused by modes of the Xbeam, Ybeams and

Xhead.

By the physical insight that the mode shapes provide, structural changes to the system can be made more efficiently. Generally, modal analysis is an easy and powerful method for retrieving a dynamic model of a structure and visualizing the mode shapes of it.

7.1 Recommendations

As a continuation and extension of this project the following recommendations for further research are given:

- The oscillations in the measured FRFs when using modal windows are likely to be caused by the modal force window. It is recommended that the nature and origin of this phenomenon are investigated in order to reduce the influence and obtain better results for lower frequencies.
- On the H-drive only two measurement points are possible for the x direction of the Xbeam. Hammer excitation of the Xbeam in x direction is not possible due to the limited space between the Xbeam and Ybeams. The accelerometer only fits in between these parts at two locations. These locations are the only two measurement points possible. With a small accelerometer more measurement points are possible. It is recommended that the response of the Xbeam is measured at more points in x direction in order to visualize the modes of the Xbeam in x direction. For example by using other sensors.
- The first two eigenmodes present in the servo FRF limit the performance of the controlled system. The mode shapes provide physical insight in these eigenmodes. With the knowledge of the mode shapes, ways to optimize the system can be found in order to manipulate the eigenmodes present in the servo FRF and to improve the performance. Examples are adjusting the inertia and stiffness of the system or adding an extra actuator at a smart position which can control certain eigenmodes of the system.

Bibliography

- [1] H. van der Auweraer. *Structural Dynamics Modeling using Modal Analysis: Applications, Trends and Challenges*. IEEE Instrumentation and Measurement, Tech., 2001.
- [2] T.G. Beckwith, R.D. Marangoni, and J.H. Lienhard. *Mechanical Measurements*. Addison Wesley Publishing Company Inc., fifth edition, 1995. ISBN 0-201-56947-7.
- [3] F. Behi and D. Tesar. *Parametric Identification for Industrial Manipulators Using Experimental Modal Analysis*. IEEE Transactions on Robotics and Automation, 1991.
- [4] P. Denbigh. *System Analysis & Signal Processing*. Addison Wesley Longman Ltd, 1998. ISBN 0-201-17860-5.
- [5] R.F. Jacobus and M.A. Serna. *Modal Analysis of a Three Dimensional Flexible Robot*. IEEE, 1994.
- [6] J.J. Kok and M.J.G. van de Molengraft. *Signaalanalyse, 2002/2003*. lecture notes course nr. 4A250.
- [7] B. de Kraker. *A Numerical-Experimental Approach in Structural Dynamics*, 2000. lecture notes nr. 4784.
- [8] N.M.M. Maia and J.M.M. Silva. *Theoretical and Experimental Modal Analysis*. Research Studies Press LTD., 1998. ISBN 0-86380-208-7.
- [9] M.H. Richardson and D.L. Formenti. *Global Curve Fitting of Frequency Response Measurements using the Rational Fraction Polynomial Method*. 1985. Structural Measurement Systems, Presented at 3RD IMAC Conference, Orlando, FL.
- [10] B.J. Schwarz and M.H. Richardson. *Experimental modal analysis*. Vibrant Technology, Inc., 1999.
- [11] H.M.J.R. Soemers, E.W. Gaal, H. Cox, and J. van Eijk. *The Mechatronic Design Approach, A Case Study*. CFT Philips, The Netherlands.
- [12] A.J. van der Voort. *LPV Control, Based on a Pick And Place Unit*. Master's thesis, Eindhoven University of Technology, May 2002. DCT nr. 2002-31.
- [13] Vibrant Technology Inc. *ME'scopeVES Operating Manual*, 2001.
- [14] DSP Technology Inc. *SigLab User Guide*, 1998.

Appendix A

Coordinates beam structure

The coordinates of the measurement points of the beam structure are used for the visualization of the mode shapes in ME'scope, they can be found in Table A. The directions of the reference frame can be seen in Fig. 4.2. The origin of this reference frame is placed in the middle on top of the beam. For the z measurements the accelerometer is placed at point 39 and the excitation takes place at points 1 up to 29. For the y measurements the accelerometer is placed at point 40 and the excitation is performed at points 30 up to 38.

<i>Position</i>	<i>x</i>	<i>y</i>	<i>z</i>
1	-0.25	0	0.015
2	-0.1870	0	0
3	-0.1250	0	0.015
4	-0.0625	0	0
5	0	0	0.015
6	0.0625	0	0
7	0.125	0	0.015
8	0.1870	0	0
9	0.25	0	0.015
10	-0.256	0.0125	0.015
11	-0.244	0.0125	0.015
12	-0.256	-0.0125	0.015
13	-0.244	-0.0125	0.015
14	-0.131	0.0125	0.015
15	-0.119	0.0125	0.015
16	-0.131	-0.0125	0.015
17	-0.1190	-0.0125	0.015
18	-0.0063	0.0125	0.015
19	0.0063	0.0125	0.015
20	-0.0063	-0.0125	0.015
21	0.0063	-0.0125	0.015
22	0.119	0.0125	0.015
23	0.131	0.0125	0.015
24	0.119	-0.0125	0.015
25	0.131	-0.0125	0.015
26	0.244	0.0125	0.015
27	0.256	0.0125	0.015
28	0.244	-0.0125	0.015
29	0.256	-0.0125	0.015
30	-0.25	0	0
31	-0.187	0	0
32	-0.125	0	0
33	-0.0625	0	0
34	0	0	0
35	0.0625	0	0
36	0.125	0	0
37	0.187	0	0
38	0.25	0	0
39	-0.1	0.0125	0
40	-0.1	0.05	0

Table A.1: coordinates measurement points beam structure

Appendix B

Modal parameters beam structure

This appendix contains the modal parameters of the beam structure of both the fits on the z measurements and the y measurements. The residues of these modal parameters are scaled to Unit Modal Mass using the driving point measurements.

B.1 Z direction

For the z direction the modal frequencies and modal damping can be found in Table B.1. The residues that result in the second fitting step are shown for the z direction in Table B.2 and in Table B.3.

<i>Shape</i>	<i>Frequency [Hz]</i>	<i>Damping [%]</i>
1	177	3.06
2	326	0.97
3	372	0.646
4	608	0.586
5	711	0.283
6	818	0.734

Table B.1: frequency and damping resonances z direction

<i>DOF</i>	<i>Shape 1</i>		<i>Shape 2</i>		<i>Shape 3</i>	
	Magnitude	Phase	Magnitude	Phase	Magnitude	Phase
1z	707	87.9	477	93.1	207	101
2z	281	250	1640	255	81.1	270
3z	777	279	1370	271	78.7	95.3
4z	686	273	789	77.6	49.1	267
5z	45.4	278	1910	89.5	7.27	242
6z	695	96.8	784	80.5	28.1	278
7z	760	97.6	1380	267	109	279
8z	299	73.3	1660	257	45.6	84.4
9z	630	270	335	92.8	149	72.6
10z	897	77.9	754	88.3	1560	264
11z	632	98.1	208	115	1610	271
12z	850	78.1	697	87.9	1600	85.5
13z	627	91.8	209	106	1530	90.5
14z	711	273	1400	267	1170	272
15z	767	274	1050	266	979	270
16z	739	270	1400	263	1010	89.7
17z	780	273	1090	266	1050	91.5
18z	57	273	1840	80	25.8	294
19z	120	83.6	1830	80.3	30.3	277
20z	73.9	275	1860	84.7	15.2	142
21z	94.1	96.7	1900	88.5	9.01	154
22z	792	82.4	1090	262	1200	82.1
23z	742	79.1	1400	259	1070	80.7
24z	789	78.1	1060	256	1090	260
25z	765	73.4	1420	254	1100	261
26z	671	236	258	94.9	1440	74.9
27z	876	246	826	79.4	1490	81.2
28z	666	247	283	93.1	1660	264
29z	889	239	813	79.8	1600	261
-39z	811	87.5	547	85.8	950	86.9

Table B.2: residues resonances z direction

<i>DOF</i>	<i>Shape 4</i>		<i>Shape 5</i>		<i>Shape 6</i>	
	Magnitude	Phase	Magnitude	Phase	Magnitude	Phase
1z	238	36	377	282	925	67.6
2z	4070	85.5	150	81.5	4940	88.7
3z	180	218	37.1	129	2150	267
4z	3930	268	201	262	1670	267
5z	322	289	285	122	2770	90.7
6z	3950	89.9	34.6	230	1880	269
7z	94.8	115	82.4	111	2190	272
8z	3960	266	156	83.7	5000	88.4
9z	552	270	282	58.9	1590	94.5
10z	547	284	2600	88.2	369	307
11z	989	80.8	2660	90.7	2190	84.4
12z	489	290	2720	270	320	350
13z	872	77.7	2570	273	2110	83
14z	311	110	1080	270	1850	269
15z	1120	266	915	268	3200	269
16z	328	109	872	91.8	1800	266
17z	979	266	941	92.8	3010	269
18z	530	277	2900	265	2920	89.3
19z	720	84.1	2990	265	2870	89.2
20z	563	277	3520	91.1	2730	90.5
21z	681	84.3	3280	93.2	2730	93
22z	879	93.6	1100	266	2960	271
23z	489	261	880	266	1610	274
24z	969	89.7	911	86.8	3200	270
25z	197	255	928	89.5	2190	270
26z	811	263	2460	79.4	2060	92.9
27z	697	84.3	2590	84.6	553	250
28z	835	265	2730	269	2160	95.2
29z	629	83.8	2810	266	324	236
-39z	2830	86.8	1240	87	4150	87.4

Table B.3: residues resonances z direction

B.2 Y direction

For the y direction the modal frequencies and damping is shown in Table B.4. The residues of the fitted modes in y direction can be found in Table B.5.

<i>Shape</i>	<i>Frequency [Hz]</i>	<i>Damping [%]</i>
1	500	1.65
2	502	0.293

Table B.4: frequency and damping resonances y direction

<i>DOF</i>	<i>Shape 1</i>		<i>Shape 2</i>	
	Magnitude	Phase	Magnitude	Phase
30y	1.18E+04	350	32.2	154
31y	2.89E+03	352	8.34E+00	162
32y	4.65E+03	169	1.29E+01	345
33y	9.27E+03	168	3.58E+01	349
34y	1.07E+04	170	5.40E+01	351
35y	9.09E+03	167	4.18E+01	349
36y	4.93E+03	162	1.43E+01	346
37y	3.08E+03	353	2.91E+00	151
38y	1.29E+04	348	4.74E+01	168
40y	337	12.3	1.58E+03	358

Table B.5: residues resonances y direction

Appendix C

Mode shapes beam structure

C.1 Shapes z direction

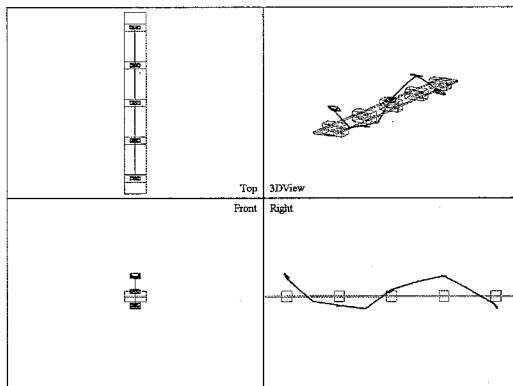


Figure C.1: 2nd bending mode in z direction at 177 Hz

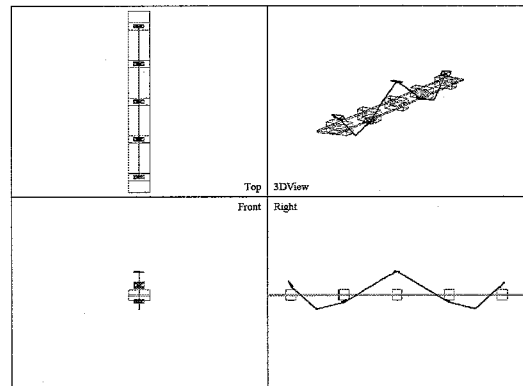


Figure C.2: 3rd bending mode in z direction at 326 Hz

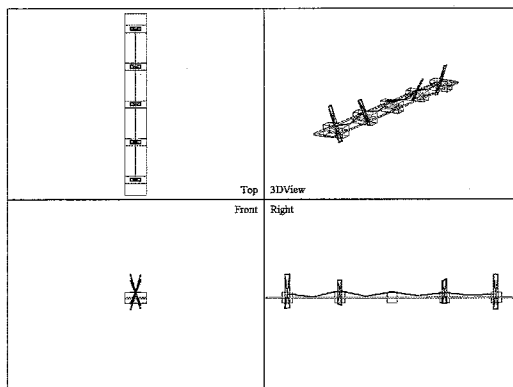


Figure C.3: 1st torsional mode in z direction at 372 Hz

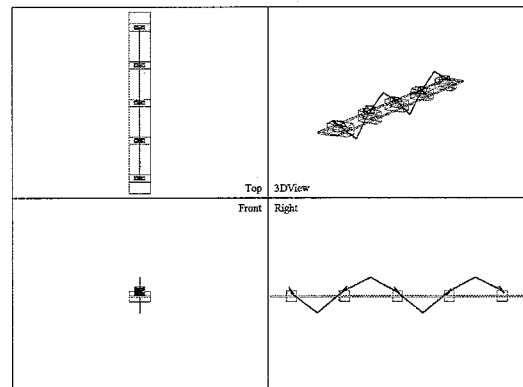


Figure C.4: 4th bending mode in z direction at 608 Hz

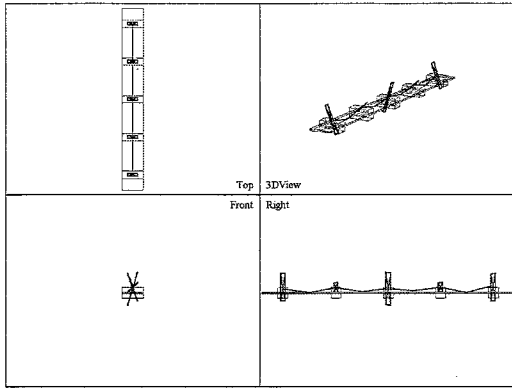


Figure C.5: 2^{nd} torsional mode in z direction at 711 Hz

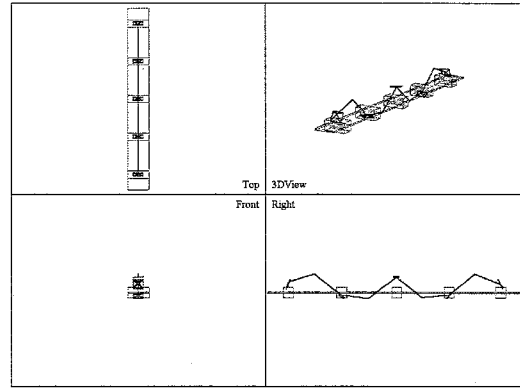


Figure C.6: 5^{th} bending mode in z direction at 818 Hz

C.2 Shapes y direction

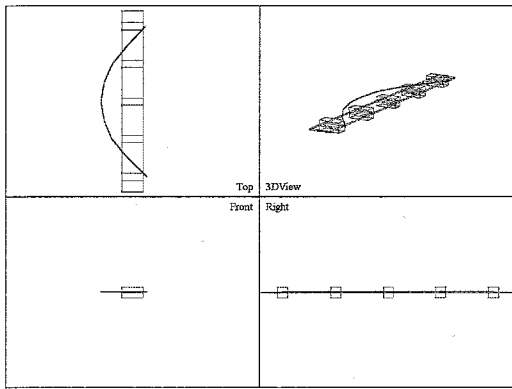


Figure C.7: 1^{st} bending mode in y direction at 500 Hz

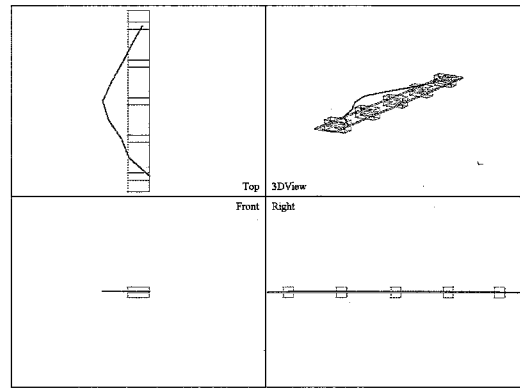


Figure C.8: folding mode in y direction at 502 Hz

Appendix D

Coordinates configuration 1

The coordinates of the measurement points of the H-drive can be used in a structure file in ME'scope to visualize the mode shapes. The tables in the sections below give the coordinates of the measurement points of the different parts.

D.1 Coordinates Xbeam

<i>Position</i>	<i>x</i>	<i>y</i>	<i>z</i>
1	-0.69	0.715	0
2	-0.63	0.715	0
3	-0.57	0.715	0
4	-0.51	0.715	0
5	-0.45	0.715	0
6	-0.39	0.715	0
7	-0.33	0.715	0
8	-0.27	0.715	0
9	-0.21	0.715	0
10	-0.15	0.715	0
11	-0.09	0.715	0
12	-0.03	0.715	0
13	0.03	0.715	0
14	0.09	0.715	0
15	0.15	0.715	0
16	0.15	0.915	0
17	0.09	0.915	0

<i>Position</i>	<i>x</i>	<i>y</i>	<i>z</i>
18	0.03	0.915	0
19	-0.03	0.915	0
20	-0.09	0.915	0
21	-0.15	0.915	0
22	-0.21	0.915	0
23	-0.27	0.915	0
24	-0.33	0.915	0
25	-0.39	0.915	0
26	-0.45	0.915	0
27	-0.51	0.915	0
28	-0.57	0.915	0
29	-0.63	0.915	0
30	-0.69	0.915	0
31	-0.12	0.72	0
83	0.21	0.905	-0.06
84	-0.75	0.905	-0.06

Table D.1: coordinates measurement points Xbeam

D.2 Coordinates Xhead

<i>Position</i>	<i>x</i>	<i>y</i>	<i>z</i>
66	-0.382	0.715	0.055
67	-0.382	0.715	0.025
68	-0.158	0.715	0.055
69	-0.158	0.715	0.025
70	-0.158	0.915	0.055
71	-0.158	0.915	0.025
72	-0.382	0.915	0.055
73	-0.382	0.915	0.025
74	-0.158	0.885	0.035

<i>Position</i>	<i>x</i>	<i>y</i>	<i>z</i>
75	-0.382	0.715	0.04
76	-0.158	0.715	0.04
77	-0.158	0.915	0.04
78	-0.382	0.915	0.04
79	-0.372	0.715	0.065
80	-0.168	0.715	0.065
81	-0.168	0.915	0.065
82	-0.372	0.915	0.065

Table D.2: coordinates measurement points Xhead

D.3 Coordinates Ybeam

<i>Position</i>	<i>x</i>	<i>y</i>	<i>z</i>
32	-0.765	-0.24	-0.055
33	-0.765	-0.14	-0.055
34	-0.765	-0.04	-0.055
35	-0.765	0.06	-0.055
36	-0.765	0.16	-0.055
37	-0.765	0.26	-0.055
38	-0.765	0.36	-0.055
39	-0.765	0.46	-0.055
40	-0.765	0.56	-0.055
41	-0.765	0.66	-0.055
42	-0.765	0.76	-0.055
43	-0.765	0.86	-0.055
44	-0.765	0.96	-0.055
45	-0.765	1.06	-0.055
46	-0.765	1.16	-0.055
47	-0.765	1.26	-0.055
48	-0.765	0.31	-0.045

<i>Position</i>	<i>x</i>	<i>y</i>	<i>z</i>
49	0.225	-0.24	-0.055
50	0.225	-0.14	-0.055
51	0.225	-0.04	-0.055
52	0.225	0.06	-0.055
53	0.225	0.16	-0.055
54	0.225	0.26	-0.055
55	0.225	0.36	-0.055
56	0.225	0.46	-0.055
57	0.225	0.56	-0.055
58	0.225	0.66	-0.055
59	0.225	0.76	-0.055
60	0.225	0.86	-0.055
61	0.225	0.96	-0.055
62	0.225	1.06	-0.055
63	0.225	1.16	-0.055
64	0.225	1.26	-0.055
65	0.225	0.31	-0.045

Table D.3: coordinates measurement points Ybeam

D.4 Coordinates Yhead

<i>Position</i>	<i>x</i>	<i>y</i>	<i>z</i>
85	-0.968	0.935	0.005
86	-0.968	0.875	0.005
87	-0.968	0.755	0.005
88	-0.968	0.695	0.005
89	-0.787	0.94	0.015
90	-0.817	0.94	0.015
91	-0.847	0.94	0.015
92	-0.877	0.94	0.015
93	-0.907	0.94	0.015
94	-0.817	0.69	0.015

<i>Position</i>	<i>x</i>	<i>y</i>	<i>z</i>
95	0.428	0.695	0.005
96	0.428	0.755	0.005
97	0.428	0.875	0.005
98	0.428	0.935	0.005
99	0.247	0.94	0.015
100	0.277	0.94	0.015
101	0.307	0.94	0.015
102	0.337	0.94	0.015
103	0.367	0.94	0.015
104	0.277	0.69	0.015

Table D.4: coordinates measurement points Yhead

Appendix E

Coordinates configuration 2

Since only the Xhead changed position, the only coordinates that change are the coordinates of the measurement points of the Xhead. Only these new coordinates will be presented in this appendix. The other coordinates are the same as for configuration 1 and can be found in Appendix D.

E.1 Coordinates Xhead

<i>Position</i>	<i>x</i>	<i>y</i>	<i>z</i>
66	-0.622	0.715	0.055
67	-0.622	0.715	0.025
68	-0.398	0.715	0.055
69	-0.398	0.715	0.025
70	-0.398	0.915	0.055
71	-0.398	0.915	0.025
72	-0.622	0.915	0.055
73	-0.622	0.915	0.025
74	-0.398	0.885	0.035

<i>Position</i>	<i>x</i>	<i>y</i>	<i>z</i>
75	-0.622	0.715	0.04
76	-0.398	0.715	0.04
77	-0.398	0.915	0.04
78	-0.622	0.915	0.04
79	-0.612	0.715	0.065
80	-0.408	0.715	0.065
81	-0.408	0.915	0.065
82	-0.612	0.915	0.065

Table E.1: coordinates measurement points Xhead

Appendix F

Modal parameters H-drive conf 1

This appendix contains the modal parameters of the H-drive of the fits on the various parts. The residues of these modal parameters are scaled to unit modal mass using the driving point measurements, except for the x direction of the Xbeam, since for this set of measurements no driving point measurement exists.

F.1 X direction Xbeam

<i>Shape</i>	<i>Frequency [Hz]</i>	<i>Damping [%]</i>
1	157	3.17
2	246	2.67
3	286	0.372

Table F.1: frequency and damping x direction Xbeam

<i>DOF</i>	<i>Shape 1</i>		<i>Shape 2</i>		<i>Shape 3</i>	
	Magnitude	Phase	Magnitude	Phase	Magnitude	Phase
83x/13z	1.26	347	2.69	277	0.404	169
83x/18z	1.51	345	1.08	308	0.328	170
83x/1z	1.35	188	1.84	71.9	0.463	9.43
83x/26z	0.417	188	1.35	53.9	0.357	19.3
83x/30z	0.86	211	1.45	84.1	0.439	12.9
83x/ 5z	0.355	156	1.22	70.2	0.328	10.1
-84x/13z	1.54	167	2.71	98.5	0.472	346
-84x/18z	1.84	171	1.32	112	0.37	349
-84x/1z	1.67	360	1.73	256	0.504	185
-84x/26z	0.409	320	1.37	245	0.356	193
-84x/30z	0.86	14.3	0.918	255	0.427	192
-84x/5z	0.608	330	1.37	245	0.41	188

Table F.2: residues x direction Xbeam

F.2 Y and z direction Xbeam

<i>Shape</i>	<i>Frequency [Hz]</i>	<i>Damping [%]</i>
1	112	3.82
2	301	0.518

Table F.3: frequency and damping y and z direction Xbeam

<i>DOF</i>	<i>Shape 1</i>		<i>Shape 2</i>	
	Magnitude	Phase	Magnitude	Phase
11z	66.1	47	89.3	36.5
13z	63.4	48.7	127	35.1
15z	61.7	49.4	123	34.2
16y	46	215	11.4	227
16z	57.8	236	109	24.8
18y	47.1	217	6.1	242
18z	72	223	132	18.9
1z	70.4	44.3	152	204
20y	44.2	219	4.26	283
20z	83	219	103	20.3
23y	45.6	216	7.24	322
23z	104	217	12.1	348
26y	52.2	214	6.31	337
26z	82.8	222	95.2	209
28y	57.7	217	4.65	332
28z	67.3	225	141	208
30y	61.5	220	5.39	25.3
30z	59.3	224	141	212
31z	83	31.3	90.8	37.9
3z	82.8	48.4	135	203
5z	93.3	54.2	102	197
8z	87.2	56.1	17.3	119
-11y	30.8	50.1	8.48	82.8
-13y	35.3	39.8	10.6	70.5
-15y	44.2	50	19	55.9
-1y	54.4	47.2	13.5	224
-3y	49.8	41.1	11	210
-5y	42	41.5	8.06	187
-8y	33.2	40.1	6.22	122

Table F.4: residues y and z direction Xbeam

F.3 Xhead

<i>Shape</i>	<i>Frequency [Hz]</i>	<i>Damping [%]</i>
1	159	5.21
2	452	0.555

Table F.5: frequency and damping Xhead

<i>DOF</i>	<i>Shape 1</i>		<i>Shape 2</i>	
	Magnitude	Phase	Magnitude	Phase
68x	261	355	149	246
69x	298	353	217	248
70x	245	0.157	29.1	5.77
70y	6.67	87.4	72.6	276
71x	261	2.83	59.7	327
71y	4.22	96.4	66.1	269
72y	5.37	138	131	70.8
73y	4.96	102	105	79
74x	267	359	52.4	322
76x	307	345	183	243
77x	246	6.28	45.2	337
77y	4.5	124	69.7	275
78y	5.72	118	119	71.2
-66x	260	182	159	79.5
-66y	10.7	359	135	253
-67x	299	177	196	83
-67y	7.03	354	103	265
-68y	9.97	3.09	58.1	67
-69y	3.89	34.8	71.9	72.5
-72x	267	175	30	185
-73x	307	165	58.5	154
-75x	285	180	184	81
-75y	7.29	350	115	259
-76y	6.05	12.1	73.9	76.3
-78x	318	161	34.4	163

Table F.6: residues Xhead

F.4 Y1beam

<i>Shape</i>	<i>Frequency [Hz]</i>	<i>Damping [%]</i>
1	79.6	1.84
2	225	1.38

Table F.7: frequency and damping Y1beam

<i>DOF</i>	<i>Shape 1</i>		<i>Shape 2</i>	
	<i>Magnitude</i>	<i>Phase</i>	<i>Magnitude</i>	<i>Phase</i>
-49x	29.4	183	68	157
-51x	26	184	47.6	163
-53x	22.9	184	28.2	174
-55x	19.8	186	1.29E+01	181
-57x	1.50E+01	186	1.54	283
-61x	7.86E+00	184	1.63E+01	344
-63x	4.55	180	1.80E+01	345
-65x	1.99E+01	185	1.86E+01	172

Table F.8: residues Y1beam

F.5 Y2beam

<i>Shape</i>	<i>Frequency [Hz]</i>	<i>Damping [%]</i>
1	79.5	1.99
2	225	1.44

Table F.9: frequency and damping Y2beam

<i>DOF</i>	<i>Shape 1</i>		<i>Shape 2</i>	
	<i>Magnitude</i>	<i>Phase</i>	<i>Magnitude</i>	<i>Phase</i>
34x	31	2.46	63.9	340
32x	35.6	5.19	97.1	335
36x	27.4	1.94	37.7	350
38x	24.1	1.57	1.80E+01	6
40x	1.93E+01	1.92	2.06	62.1
44x	1.08E+01	9	2.05E+01	166
46x	7.02	10.8	2.44E+01	152
48x	2.55E+01	1.45	2.23E+01	2.68

Table F.10: residues Y2beam

Appendix G

Mode shapes H-drive conf 1

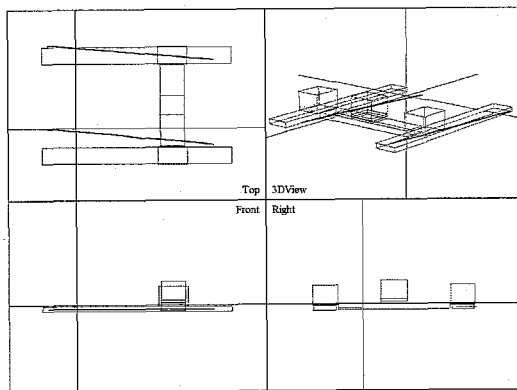


Figure G.1: one line with one end fixed mode of the Ybeam at 79.5 Hz

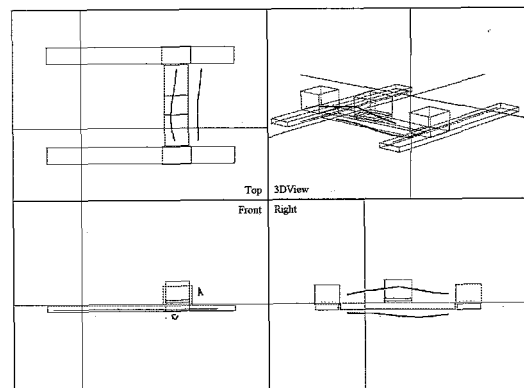


Figure G.2: swinging mode of the Xbeam at 112 Hz

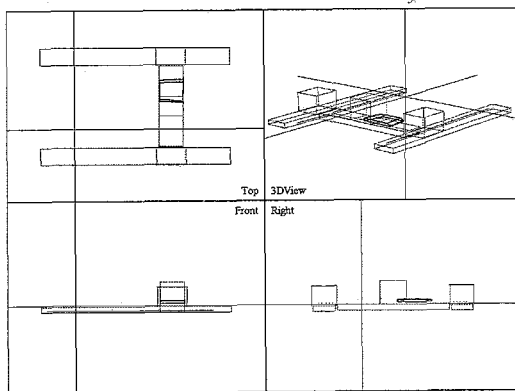


Figure G.3: translational mode of the Xhead at 159 Hz

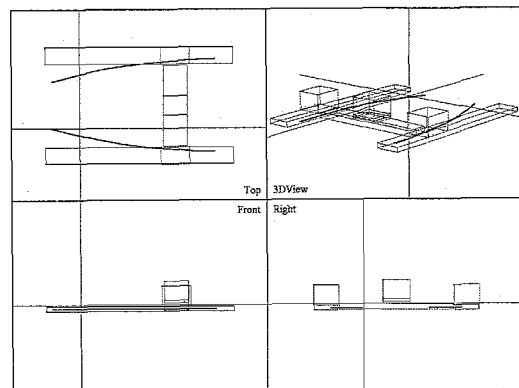


Figure G.4: curved line mode of the Ybeam at 225 Hz

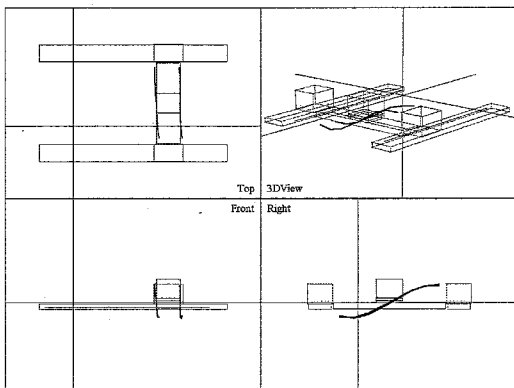


Figure G.5: 2nd bending mode of the Xbeam at 301 Hz

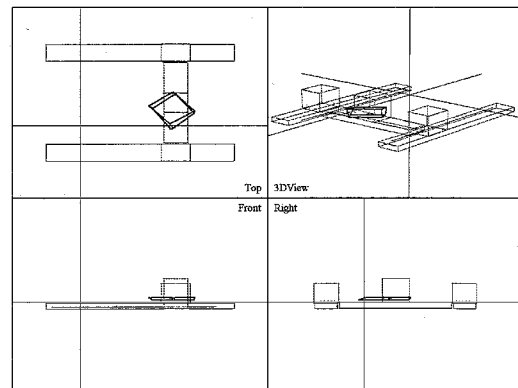


Figure G.6: turning mode of the Xhead at 452 Hz

Appendix H

Modal parameters H-drive conf 2

This appendix contains the modal parameters of the H-drive of the fits on the various parts. The residues of these modal parameters are scaled to unit modal mass using the driving point measurements, except for the x direction of the Xbeam, since for this set of measurements no driving point measurement exists.

H.1 X direction Xbeam

<i>Shape</i>	<i>Frequency [Hz]</i>	<i>Damping [%]</i>
1	156	3.58
2	248	1.68
3	279	1.31

Table H.1: frequency and damping x direction Xbeam

<i>DOF</i>	<i>Shape 1</i>		<i>Shape 2</i>		<i>Shape 3</i>	
	Magnitude	Phase	Magnitude	Phase	Magnitude	Phase
83x/13z	1.01	331	3.62	197	7.68	115
83x/18z	1.68	337	1.47	228	5.26	123
83x/1z	2.55	142	1.71	47.5	6.03	289
83x/23z	1.09	350	0.541	257	2.54	91.7
83x/30z	1.96	150	1.19	48.5	6.3	309
83x/8z	0.134	208	1	229	3.24	116
-84x/13z	1.42	154	3.17	34.9	4.74	307
-84x/18z	1.99	159	1.6	71.1	3.8	317
-84x/1z	3.03	324	1.58	230	3.95	112
-84x/23z	1.67	170	0.511	76.4	1.31	281
-84x/30z	2.36	333	0.897	238	4.59	153
-84x/8z	0.0977	69.4	0.832	58.9	1.73	302

Table H.2: residues x direction Xbeam

H.2 Y and z direction Xbeam

<i>Shape</i>	<i>Frequency [Hz]</i>	<i>Damping [%]</i>
1	97.8	2.34
2	123	4.55
3	277	2.01

Table H.3: frequency and damping y and z direction Xbeam

<i>DOF</i>	<i>Shape 1</i>		<i>Shape 2</i>		<i>Shape 3</i>	
	Magnitude	Phase	Magnitude	Phase	Magnitude	Phase
11z	120	358	133	353	447	353
13z	90.2	359	120	349	474	353
15z	51.9	1.73	101	0.0763	357	357
16y	3.26	50.8	16.8	172	3.47	248
16z	27.1	1.33	72	196	245	354
18y	3.27	68.5	27	171	4.15	265
18z	60.1	359	91.6	185	344	350
1z	81.1	356	132	354	342	164
20y	3.54	68.3	36.8	171	6.74	299
20z	88.8	359	104	184	349	349
22y	4.24	75.3	38.6	163	8.46	307
22z	112	357	120	189	238	351
24y	5.4	98.6	48.9	159	8.29	301
24z	118	357	135	186	59.9	315
27y	6.09	108	70.3	157	8.69	289
27z	76.9	359	165	172	198	186
30y	9.14	143	99.2	154	11.3	320
30z	46.1	0.209	104	186	337	175
31z	130	1.73	108	359	444	356
4z	138	357	175	356	204	169
7z	147	358	163	351	103	360
9z	137	1.14	140	358	288	0.477
-11y	5.53	304	27.8	357	10.1	83.2
-13y	4.43	289	25.1	347	9.35	74.6
-15y	3.37	281	10.9	357	9.96	59.2
-1y	10.6	322	93.6	341	15.2	177
-4y	9.36	313	60	342	9.18	147
-7y	8.86	317	49.9	343	9.65	121
-9y	6.81	310	34	347	8.92	99.6

Table H.4: residues y and z direction Xbeam

H.3 Xhead

<i>Shape</i>	<i>Frequency [Hz]</i>	<i>Damping [%]</i>
1	157	6
2	473	1.68

Table H.5: frequency and damping Xhead

<i>DOF</i>	<i>Shape 1</i>		<i>Shape 2</i>	
	Magnitude	Phase	Magnitude	Phase
68x	396	358	541	314
69x	477	345	816	319
70x	303	7.77	36.7	170
70y	5.41	171	512	334
71x	359	1.03	94.9	349
71y	3.47	142	458	334
72y	5.66	170	338	154
73y	9.98	51.4	283	169
74x	328	4.76	70.3	336
76x	419	353	789	315
77x	307	8.03	43.9	6.59
77y	1.86	138	468	333
78y	2.61	146	345	169
79z	132	187	274	167
80z	25.3	203	408	350
81z	17.7	111	608	346
82z	78.5	178	316	213
-66x	356	184	665	138
-66y	23.9	17.1	500	338
-67x	388	184	832	144
-67y	37.8	28.2	469	331
-68y	11.8	1.2	432	136
-69y	4.79	342	478	134
-72x	288	191	79.1	45.9
-73x	342	186	69.6	121
-75x	375	184	726	142
-75y	44.9	29.6	467	326
-76y	4.56	347	482	133
-78x	346	185	64.9	69.8

Table H.6: residues Xhead

H.4 Y1beam

<i>Shape</i>	<i>Frequency [Hz]</i>	<i>Damping [%]</i>
1	79.4	2.25
2	224	1.55

Table H.7: frequency and damping Y1beam

<i>DOF</i>	<i>Shape 1</i>		<i>Shape 2</i>	
	Magnitude	Phase	Magnitude	Phase
-49x	33.6	171	83	150
-51x	29.2	173	51.6	155
-53x	24.3	179	32.2	166
-55x	19.2	187	14	170
-57x	15.3	182	1.94	208
-61x	7.9	176	11	322
-63x	4.72	168	14.7	312
-65x	22.7	196	19.9	188

Table H.8: residues Y1beam

H.5 Y2beam

<i>Shape</i>	<i>Frequency [Hz]</i>	<i>Damping [%]</i>
1	79.3	2.08
2	224	1.7

Table H.9: frequency and damping Y2beam

<i>DOF</i>	<i>Shape 1</i>		<i>Shape 2</i>	
	Magnitude	Phase	Magnitude	Phase
32x	39.5	0.706	117	333
34x	34.2	359	73	330
36x	29.9	360	44.7	339
38x	24.8	359	20.7	350
40x	20.3	0.739	3.43	120
44x	11.4	2.92	17.4	146
46x	7.25	4.33	26.7	145
48x	25.9	360	26.8	355

Table H.10: residues Y2beam

Appendix I

Mode shapes H-drive conf 2

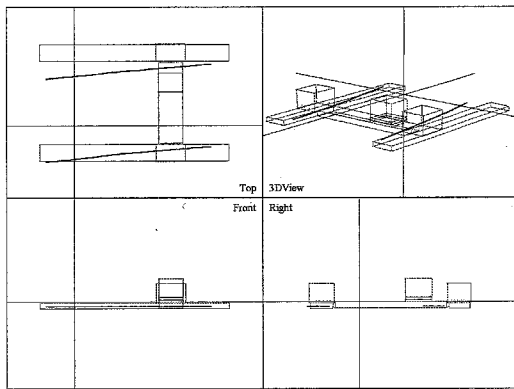


Figure I.1: one line with one end fixed mode of the Ybeam at 79.4 Hz

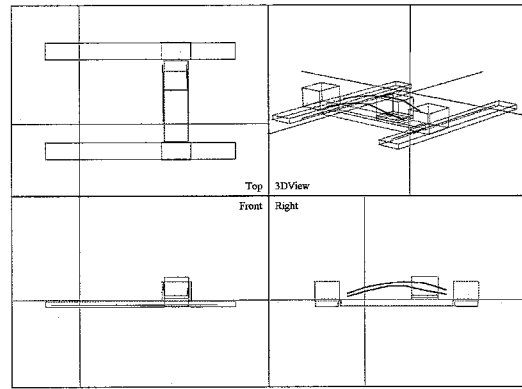


Figure I.2: 1st bending mode of the Xbeam at 97.8 Hz

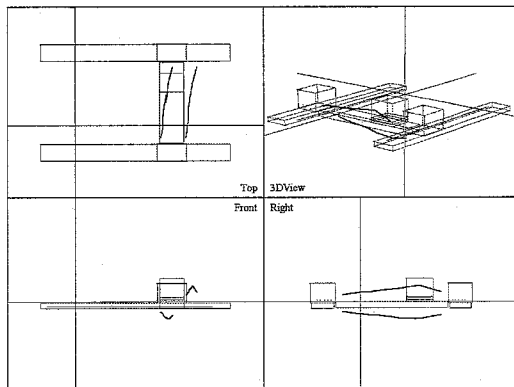


Figure I.3: swinging mode of the Xbeam at 123 Hz

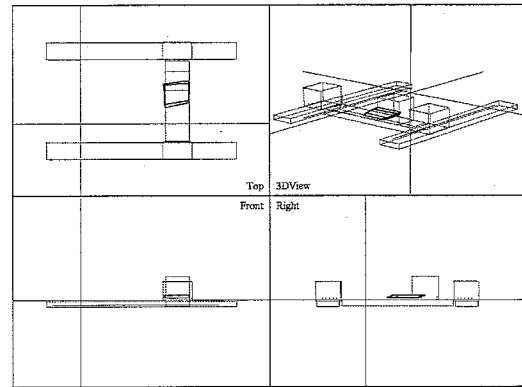


Figure I.4: translational mode of the Xhead at 157 Hz

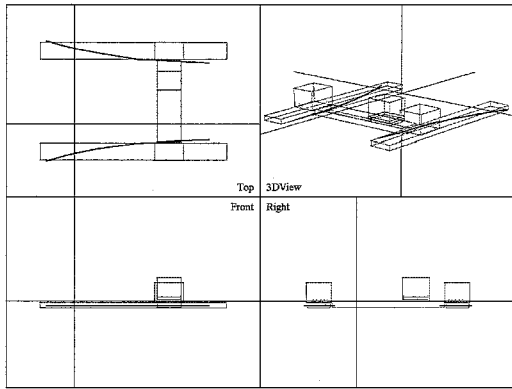


Figure I.5: curved line mode of the Ybeam at 224 Hz

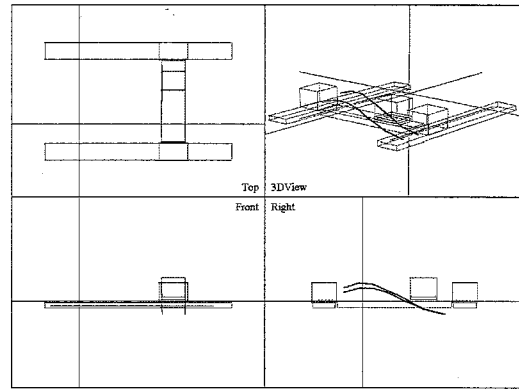


Figure I.6: 2nd bending mode of the Xbeam at 277 Hz

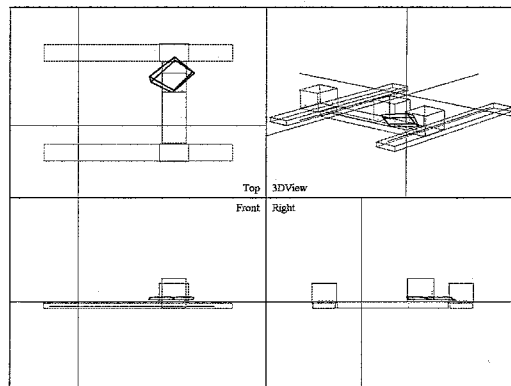


Figure I.7: turning mode of the Xhead at 473 Hz